



Research article

Identification of dual-target isoxazolidine-isatin hybrids with antidiabetic potential: Design, synthesis, *in vitro* and multiscale molecular modeling approaches

Siwar Ghannay^a, Budur Saleh Aldhafeeri^a, Iqrar Ahmad^b, Abuzar E.A.E. Albadri^a, Harun Patel^b, Adel Kadri^{c,d,**}, Kaiss Aouadi^{a,e,*}

^a Department of Chemistry, College of Science, Qassim University, Buraidah, 51452, Saudi Arabia

^b Division of Computer Aided Drug Design, Department of Pharmaceutical Chemistry, R. C. Patel Institute of Pharmaceutical Education and Research, Shirpur, 425405, Maharashtra, India

^c Faculty of Science and Arts in Baljurashi, Al-Baha University, P.O. Box (1988), Al-Baha, 65527, Saudi Arabia

^d Faculty of Science of Sfax, Department of Chemistry, University of Sfax, B.P. 1171, 3000, Sfax, Tunisia

^e Department of Chemistry, Laboratory of Heterocyclic Chemistry Natural Product and Reactivity/CHPNR, Faculty of Science of Monastir, University of Monastir, Avenue of the Environment, Monastir, 5019, Tunisia

ARTICLE INFO

Keywords:

Diabetes

Antidiabetic agents

Isoxazolidine-isatin hybrids

Kinetic study

Drug-likeness

Molecular docking and dynamics simulation

ABSTRACT

In the development of novel antidiabetic agents, a novel series of isoxazolidine-isatin hybrids were designed, synthesized, and evaluated as dual α -amylase and α -glucosidase inhibitors. The precise structures of the synthesized scaffolds were characterized using different spectroscopic techniques and elemental analysis. The obtained results were compared to those of the reference drug, acarbose ($IC_{50} = 296.6 \pm 0.825 \mu M$ for α -amylase & $IC_{50} = 780.4 \pm 0.346 \mu M$ for α -glucosidase). Among the title compounds, **5d** exhibited impressive α -amylase and α -glucosidase inhibitory activity with IC_{50} values of $30.39 \pm 1.52 \mu M$ and $65.1 \pm 3.11 \mu M$, respectively, followed by **5h** ($IC_{50} = 46.65 \pm 2.3 \mu M$; $IC_{50} = 85.16 \pm 4.25 \mu M$) and **5f** ($IC_{50} = 55.71 \pm 2.78 \mu M$; $IC_{50} = 106.77 \pm 5.31 \mu M$). Mechanistic studies revealed that the most potent derivative **5d** bearing the chloro substituent attached to the oxoindolin-3-ylidene core, and acarbose, are a competitive inhibitors of α -amylase and α -glucosidase, respectively. Structure activity relationship (SAR) was examined to guide further structural optimization of the most appropriate substituent(s). Moreover, drug-likeness qualities and ADMET prediction of the most active analogue, **5d** was also performed. Subsequently, **5d** was subjected to molecular docking and dynamic simulation during the progression of 120 ns analysis to check the essential ligand-receptor patterns, and to estimate its stability. *In silico* studies were found in good agreement with the *in vitro* enzymatic inhibitions results. In conclusion, we demonstrated that most potent compound **5d** could be exploited as dual potential inhibitor of α -amylase and α -glucosidase for possible management of diabetes.

* Corresponding author. Department of Chemistry, College of Science, Qassim University, Buraidah, 51452, Saudi Arabia.

** Corresponding author. Faculty of Science and Arts in Baljurashi, Al-Baha University, P.O. Box (1988), Al-Baha, 65527, Saudi Arabia.

E-mail addresses: lukadel@yahoo.fr (A. Kadri), K.AOUADI@qu.edu.sa (K. Aouadi).

<https://doi.org/10.1016/j.heliyon.2024.e25911>

Received 24 November 2023; Received in revised form 8 January 2024; Accepted 5 February 2024

Available online 11 February 2024

2405-8440/© 2024 The Authors. Published by Elsevier Ltd. This is an open access article under the CC BY-NC-ND license (<http://creativecommons.org/licenses/by-nc-nd/4.0/>).

1. Introduction

Diabetes mellitus is an incurable disease that occurs when the pancreas does not produce enough insulin, or when the body is not able to use insulin effectively which is a hormone that regulates blood sugar (essential "fuel" for its functioning) [1–3]. Over the past decade, the mortality rate caused by diabetes has continued to increase, exceeding 34% [4–7]. Studies have shown that the number of diabetics is expected to increase from 171 million in 2000 to 300 million in 2025 and up to 366 million in 2030 [8,9]. The main subtypes of DM are type 1 diabetes (T1DM), type 2 diabetes (T2DM) and gestational diabetes (G1DM) [10]. In all three cases, without treatment, the sugar level rises in the blood [11,12]. Hyperglycemia, also called high blood sugar, is a common effect of uncontrolled diabetes that, over time, causes severe damage to many body systems, especially nerves and blood vessels [13–16]. More than 65% of people with diabetes die from the disease with T2DM (Noninsulin-dependent diabetes mellitus) accounting for more than 90% is by far the most often prominent of them, which results from the combination of genetic factors, environmental and lifestyle factors [17–19]. Controlling (retarding, regulating and/or inhibiting) the post-prandial hyperglycemia by inhibiting the breakdown of carbohydrates into glucose or promoting the conversion of glucose remains is one of the best strategies for the effective treatment of type 2 diabetes [20–24]. Conventionally, α -amylase is used in the hydrolysis of long-chain of α -1,4-glycosidic linkage starch to smaller oligosaccharides and α -glucosidase expressed in the small intestine and typically cleaves the glucosidic bonds of oligosaccharides and polysaccharides into glucose units [25–27]. In this context, one of the most attractive chemotherapeutic strategies for the treatment of DM is the prevention of the reaction of pancreatic α -amylase and intestinal α -glucosidase, that blunt postprandial blood glucose [28–31]. Currently, clinically approved inhibitors of α -amylase and α -glucosidase enzymes are acarbose, miglitol and voglibose [32,33]. Meanwhile, these drugs possess various adverse effects including stress, allergic reactions, gastrointestinal disturbances, infections, flatulence, and diarrhea and therefore being side effect-prone [34–37]. This has encouraged scientists to exert much efforts in designing and developing most potent, effective and safe dual α -glucosidase and α -amylase inhibitors. A considerable number of heterocycles has been identified as potential antidiabetics such as isatin and isoxazolidine derivatives. Indeed, isatin (indoline-2,3-dione) is known for its various biological activities [38]. In Fig. 1, a previous studies have shown that structural modification at different positions of isatin makes it possible to improve its pharmacological properties, conferring it antitubercular [39,40], anti-malarial [41–43], anticonvulsant [44–46] antimicrobial [47–49], anticancer [50,51], antidiabetic [52–55] and anti-HIV [56–58] properties as well as CDK2 (cyclin-dependent kinase 2) inhibitors [59,60].

In this regard, isatin derivatives have gained the passion of many researchers owing to their broad spectrum of biological activities. For many years, our research team has focused on the identification of new biologically active biomolecules/small molecules with promising biological activities [61–70], mainly those α -amylase and α -glucosidase inhibitors [71–76]. In this context, our work has been devoted to the design and the synthesis of isoxazolidine-isatin hybrids for more potent, selective α -glucosidase and α -amylase inhibitors. Moreover, *in silico* studies were performed to gain insight into the interaction of the compounds with the active site of α -amylase and α -glucosidase enzymes.

2. Results and discussion

2.1. Chemistry

Hydrazide 4 was synthesized in three steps with an overall yield of 74%. the synthesis begins with a 1,3-dipolar cycloaddition between nitron 1 and alkene followed by an alkylation in the presence of ethyl chloroacetate to access compound 3. the reaction of hydrazine monohydrate with ester 3 gives the desired hydrazide [77]. The condensation of hydrazide 4 with three isatin derivatives was carried out in ethanol in the presence of a catalytic quantity of acetic acid at reflux to obtain the isoxazolidine-isatin hybrids 5a-c

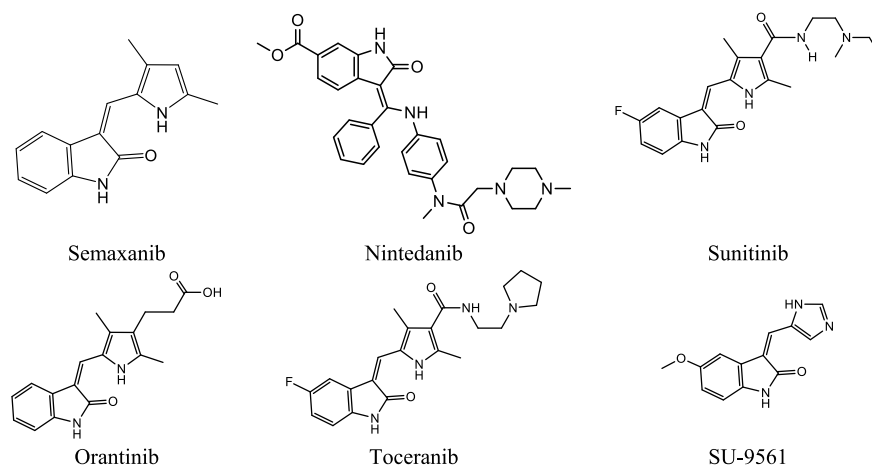


Fig. 1. Some examples of marketed isatin derivatives candidates.

(Scheme 1). Cycloadduct **6** undergoes the same arrangements as its analogue **2** to access hydrazone **8** [77]. The new isoxazoline-isatin hybrids **5d-h** are obtained by condensation of intermediate **8** with five isatin derivatives (Scheme 2).

The desired cycloadducts **2** and **6** were obtained with simultaneous creation of two asymmetric centers at C3* and C5* [77]. The stereochemistry of the final products was assigned based on 2D NOESY. Indeed, the 2D NOESY spectrum of the hybrid isoxazolidine-ization **5a** showed that the H3 and H4_{proR} protons point in the same direction. This was explained by the strong correlation observed between the H3–H4_{proR} protons. Also, the strong correlation between the H5–H4_{proS} protons and the weak NOE effect between H5–H4_{proR} confirms that the H5 and H4_{proS} protons point in the same direction. All of these observations further support the stereochemistry of the isoxazolidine-hybridization **5a** proposed in Fig. 2.

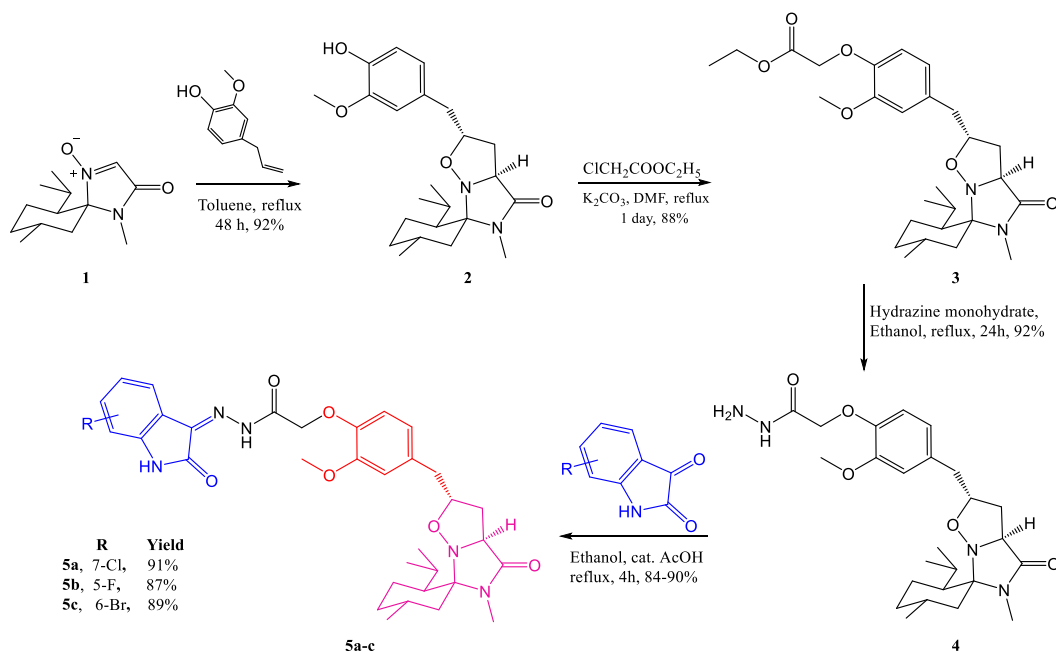
2.2. Antidiabetic profile and SAR study

Antidiabetic activity (enzymatic inhibitory effect) towards α -amylase and α -glucosidase enzymes of the newly synthesized target compounds was assessed in vitro, in the concentrations range of 10–180 μ g/mL. Acarbose was used as pharmacological standard drug for comparison with the inhibitory effects of prepared samples. Considering the results in Table 1, an excellent inhibitory activity towards both enzymes activity was detected revealing that the type of substituent and their position played a pivotal role in the inhibition activities to different extents (Fig. 3). When evaluated against a standard acarbose drug, all the newly afforded analogues showed varied ranges on α -amylase and α -glucosidase inhibitory potentials ranging from $IC_{50} = 30.39 \pm 1.52 \mu$ M to $193.83 \pm 9.54 \mu$ M and from $IC_{50} = 65.1 \pm 3.11 \mu$ M to $208.72 \pm 10.38 \mu$ M, respectively. In this series, analogue **5d** bearing the electron-withdrawing chloro (-Cl) substituent attached to the oxoindolin-3-ylidene core showed the better inhibitory profile with $IC_{50} = 30.39 \pm 1.52 \mu$ M (α -amylase) and $65.1 \pm 3.11 \mu$ M (α -glucosidase), respectively. When changing the 6-methyl group in **5d** by 4-methoxy moiety (**5a**), the activity was significantly impaired by a factor of 6.3 and 3.2, respectively towards α -amylase and α -glucosidase. Moreover, compound **5h** bearing fluoro (-F) electron-withdrawing group at C-7 on oxoindolin-3-ylidene core dispose of high antidiabetic activity against both enzymes, greater than **5f** with C-5 fluoro group, which, in turn, showed remarkable potency than **5g** bearing a methyl as electron-donating group at the same position, C-5 of oxoindolin-3-ylidene. Analogue **5e** that hold the methyl group at the 6-position of the phenoxy core and bromo group at the 6-position of oxoindolin-3-ylidene showed higher activity than **5c**, with methoxy group attached to C-4 of the phenoxy core.

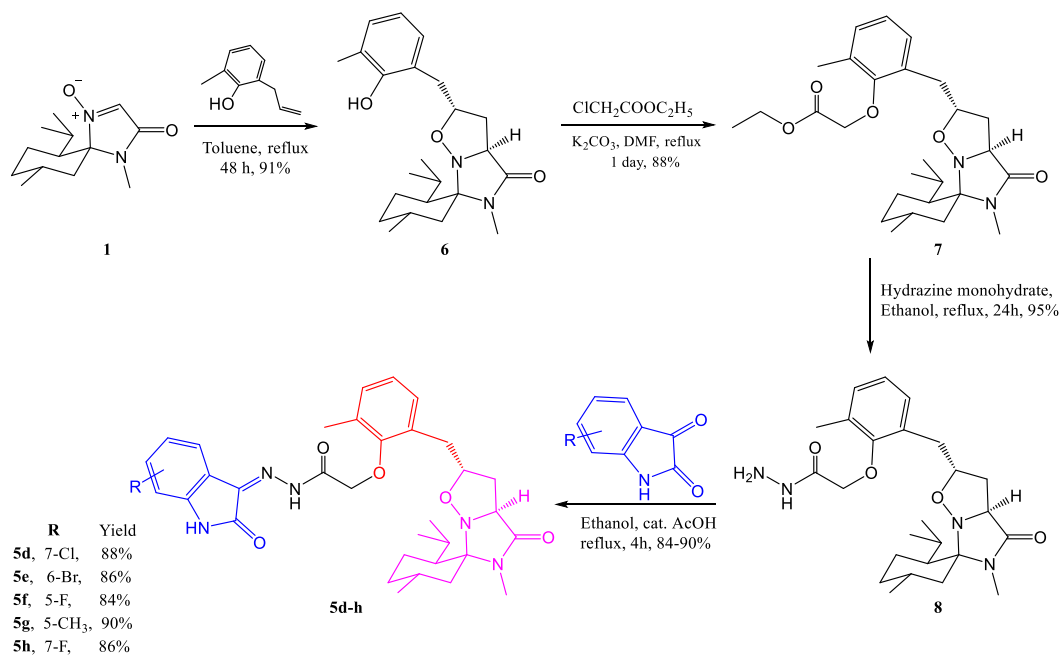
2.3. Enzymatic kinetic study

2.3.1. Inhibition mode of α -amylase by **5d** and acarbose

In order to unravel the inhibitory mechanism of the **5d** and acarbose extract on α -amylase, kinetic studies have been assessed. Our findings (Fig. 4, a and c) revealed that the intercept, maximum rate V_{max} was essentially unchanged while the Michaelis constant, K_m increased suggesting that **5d** exhibited a competitive inhibition towards α -amylase, similar to the behavior of acarbose, used as standard drug. K_i values (Fig. 4, b and d) of compound **5d** and acarbose were 27.49 μ M and 291.69 μ M, respectively meaning that they



Scheme 1. Synthesis of isoxazolidine-isatin hybrids **5a-c**.



Scheme 2. Synthesis of isoxazolidine-isatin hybrids **5d-h**.

have a greater affinity for the enzyme.

2.3.2. Inhibition mode of α -glucosidase by **5d** and acarbose

To obtain more in-depth insight into the mechanism of inhibition of **5d** and acarbose by α -glucosidase enzyme, kinetics study was performed. The Lineweaver–Burk plot (Fig. 5, a and c) showed that V_{max} values were not affected, however the K_m values increased to overcome the inhibitory effect of the competitor. The observed inhibition type revealed that **5d** and acarbose bind to the active site on the enzyme and compete with the substrate for binding to the active site. The estimation of K_i via the concentrations of **5d** and acarbose versus the slope, was found to be 56.06 μ M and 763.28 μ M, respectively.

2.4. Drug-likeness and ADMET properties

Computer-aided ADMET (absorption, distribution, metabolism, excretion, and toxicity) screening was performed for the most potent analogue **5d** to differentiate between drug-like and non-drug-like and to improve the quality control of drugs at the earliest stages in their development, using different computational approaches [78–82]. In the present work, ADMET properties of **5d** were computed using swissADME, pre-ADMET and pKCSM tools. Compound **5d** was found to not violated Lipinski's rule of five despite the molecular weights of 622.15 g/mol, with numbers of rotatable bonds of 8 (NROTB \leq 10), hydrogen-bond acceptor of 7 (HBA \leq 10), and hydrogen-bond donor of 2 (HBD \leq 5). The absorption was deduced via %Abs = $109 \pm [0.345 \times \text{TPSA}]$ revealing a value of 70.2. Lipophilicity was predicted using different algorithms. The Consensus LogPo/w descriptor of **5d** was found to be 4.53 which maximize its transportation and easily could reach the target site. Moreover, **5d** exhibited high gastrointestinal (GI) absorption, with the ability to be a substrate of P-gp and not cross the blood–brain barrier (BBB) which implies risks of CNS side effects. The metabolism of **5d** was predicted based on its behavior to inhibit cytochrome P450 (CYP) isoforms for its role in drug elimination through metabolic biotransformation. As depicted in Table 2, **5d** was found to show no inhibitory activity towards any of CYP models suggesting that it was not involved in any biotransformation process. Additionally, Swiss ADME analyses revealed that **5d** showed no violation of three filters (Lipinski, Ghose, and Muegge). The percentage of drug molecule that might reach the systemic circulation estimated by the bioavailability score was 0.55. Very low skin permeation was predicted for **5d** via LogKp (-5.52 cm/s).

Bioavailability radar for drug-likeness depiction and boiled-egg graph provide the possibility of **5d** to be easily absorbed by the GI and was actively effluxed by P-gp (PGP+). The ligand-based target prediction of **5d** has been estimated and was restricted to the top 15 Homo sapiens targets. Performed data showed that **5d** was estimated to have a 60% probability of binding kinase, 20% of binding protease and 6.7% of binding enzyme, phosphodiesterase and other ion channel.

For better reducing expenses and to gain a lot of time during the drug discovery process, The in silico reliable prediction of toxicity remains a crucial step. The toxicity level of **5d** has been predicted via their carcinogenicity and mutagenicity by determining Carcinogenicity/Mouse/Rat and AMES test, respectively. Also, hERG-inhibition was checked in order to have an idea about its cardiac toxicity as shown, **5d** displayed non-carcinogenic, non-mutagenic and non-cardiac toxicity effect as well as no skin sensitization.

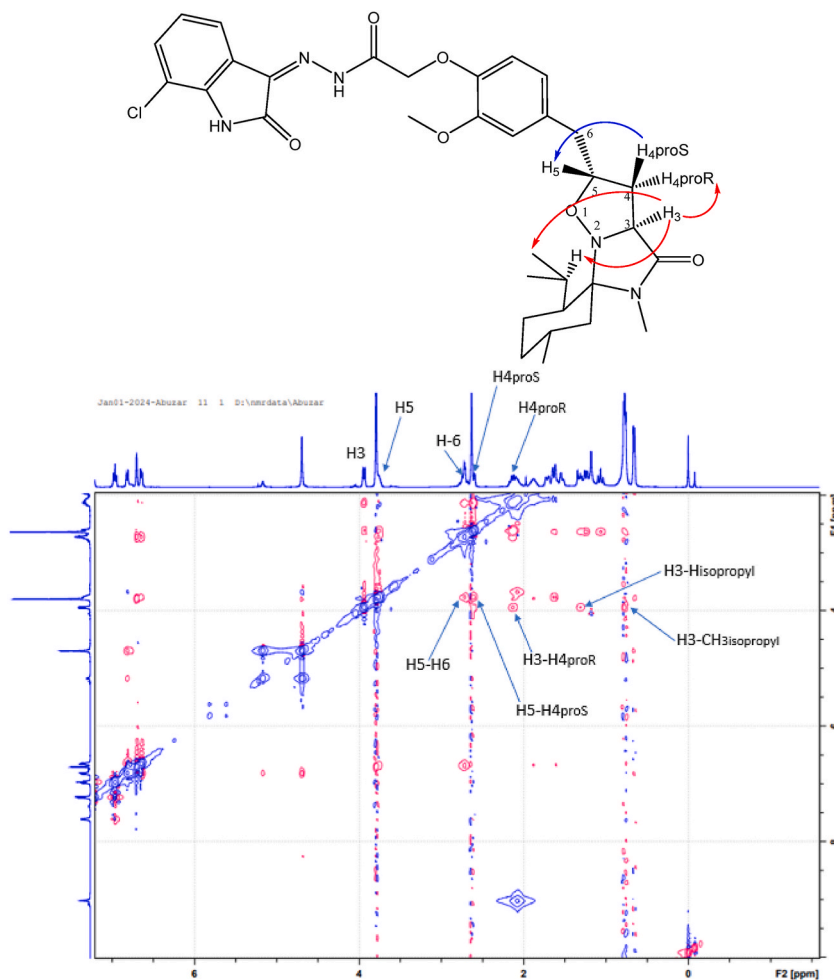


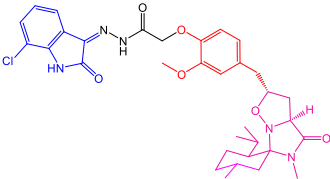
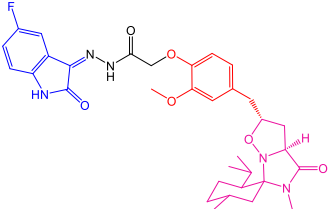
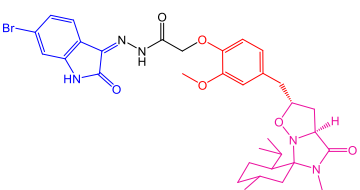
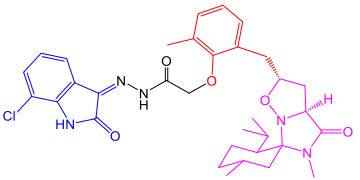
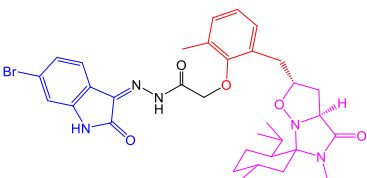
Fig. 2. NOESY spectrum and NOE effects for compound 5a.

2.5. Molecular docking study

Antidiabetic drugs are thought to be particularly effective against the α -glucosidase and α -amylase enzymes. These enzymes are important in carbohydrate metabolism because they break down complex carbohydrates into simpler forms like glucose. Therefore, the binding interaction and the binding ability at the active site of α -glucosidase enzyme and α -amylase enzyme were explored to better comprehend the observed biological activities by which the synthesized derivatives showed their antidiabetic efficacy. By reducing the activity of these enzymes, carbohydrate digestion and absorption can be delayed, resulting in a drop in postprandial glucose levels. α -glucosidase inhibitors function by inhibiting the activity of α -glucosidase in the small intestine, lowering glucose absorption. This helps to manage blood glucose levels after meals and reduces postprandial glucose increases. Similarly, α -amylase inhibitors work by inhibiting the α -amylase enzyme, which is responsible of breaking down starches into simpler sugars. Inhibiting the activity of α -amylase delays the conversion of dietary starches into glucose, resulting in improved glycemic management. Targeting both these enzymes provides a way for controlling postprandial hyperglycemia, which is a significant problem in diabetes therapy. It is feasible to limit carbohydrate digestion and absorption by designing medications that specifically block α -glucosidase and α -amylase, resulting in better glycemic control in diabetics. Table 3 summarizes the docking results of physiologically active synthesized compounds with α -glucosidase and α -amylase. For both enzymes, higher docking scores indicate stronger binding affinities. Compounds with more negative scores are likely to have better interactions with the respective enzyme's active site. In the analysis of the α -amylase enzyme, **5d** stands out as the most potent inhibitor with a docking score of -6.602 kcal/mol, followed by **5h** (-6.262 kcal/mol) and **5f** (-5.741 kcal/mol) (Table 3). The docking scores indicate strong binding affinities, with **5d** showing the highest inhibitory activity among all the listed compounds. This suggests that **5d** is the most promising compound for targeting the α -amylase enzyme. Similarly, in the evaluation of the α -glucosidase enzyme, **5d** exhibits the strongest inhibitory activity with a docking score of -5.414 kcal/mol, followed by **5h** (-5.381 kcal/mol) and **5f** (-5.102 kcal/mol). Interestingly, **5d** also demonstrates the most negative docking score among all compounds for α -glucosidase, indicating a robust binding affinity. Thus, **5d** shows significant potential as a drug candidate for targeting the α -glucosidase enzyme as well. Remarkably, **5d** appears to have the highest predicted binding affinity for both α -amylase

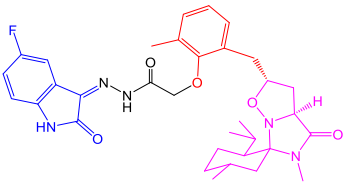
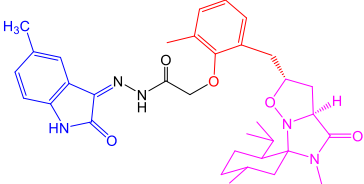
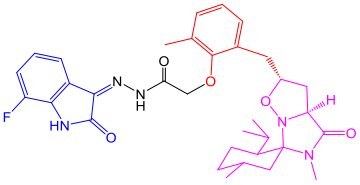
Table 1

α -Amylase and α -glucosidase inhibitory effect IC_{50} (μ M) of isoxazolidine-isatin hybrids **5a-h**. The results are expressed in mean values \pm standard error (or standard error); **5a-h**: The means of the same column with a different letter are significantly different ($P < 0.05$).

Entry	Structure	α -Amylase IC_{50} (μ M)	α -Glucosidase IC_{50} (μ M)
5a		193.83 \pm 9.54 ^g	208.72 \pm 10.38 ^f
5b		174.33 \pm 8.71 ^f	215.19 \pm 70.7 ^g
5c		68.02 \pm 3.4 ^c	152.44 \pm 7.56 ^d
5d		30.39 \pm 1.52 ^a	65.1 \pm 3.11 ^a
5e		92.44 \pm 4.05 ^d	171.88 \pm 8.44 ^e

(continued on next page)

Table 1 (continued)

Entry	Structure	α -Amylase IC ₅₀ (μ M)	α -Glucosidase IC ₅₀ (μ M)
5f		55.71 \pm 2.78 ^b	106.77 \pm 5.31 ^c
5g		134.6 \pm 6.73 ^e	218.56 \pm 40.26 ^g
5h		46.65 \pm 2.3 ^b	85.16 \pm 4.25 ^b
Acarbose		296.6 \pm 0.825	780.4 \pm 0.346

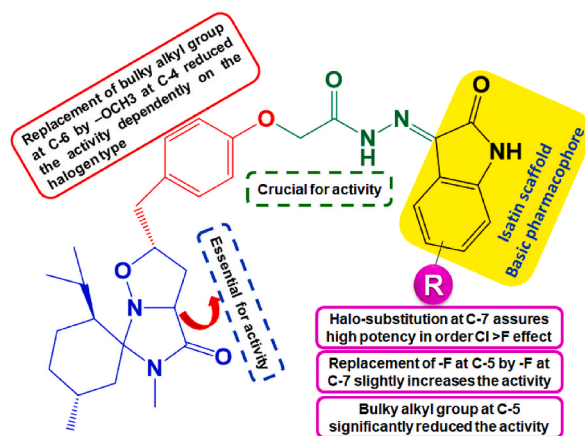


Fig. 3. SAR summary of the synthesized compounds.

(−6.602 kcal/mol) and α -glucosidase (−5.414 kcal/mol), making it an advantageous dual-target drug candidate for developing antidiabetic medications. Its ability to effectively inhibit the activity of both enzymes suggests potential benefits in diabetes management. Additionally, **5h** and **5f** show promise as candidates for targeting α -amylase and α -glucosidase, respectively, given their strong binding affinities. Moreover, **5b**, **5c**, **5f**, and **5g** demonstrate relatively promising binding affinities for both enzymes, indicating they could be further investigated as potential drug candidates for diabetes treatment.

Fig. 6 illustrates the graphical representations of the **5d**-protein interactions, employing both 2D and 3D representations. The binding analysis revealed that representative compound **5d** forms weak non-covalent interactions with these enzymes, primarily

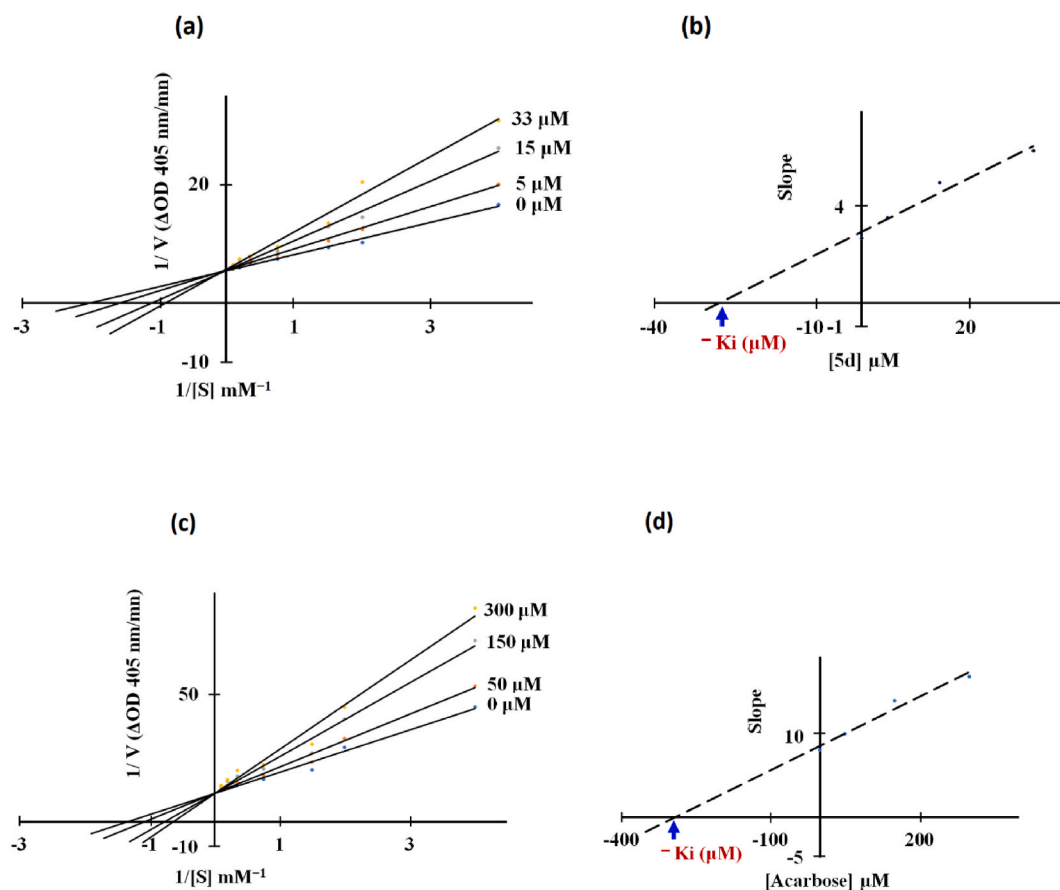


Fig. 4. (a) and (c) Lineweaver–Burk plot of the kinetics of α -amylase inhibition by **5d** and acarbose, respectively. (b) and (d) Secondary re-plot of Lineweaver–Burk plots between the slopes of each line on Lineweaver–Burk plot versus various concentrations of **5d** and acarbose, respectively.

involving hydrogen bonding and π - π interactions. In the α -amylase enzyme, **5d** establishes two significant hydrogen bond interactions with critical amino acid residues, Asp300 and Ala106. These hydrogen bonds play a vital role in stabilizing the ligand-receptor complex and contribute to the high affinity of **5d** for the active site of α -amylase. Furthermore, a notable π - π interaction is observed between the phenyl ring of **5d** and Trp59, further enhancing the compound's binding and positioning within the enzyme's active site (Fig. 6A). Similarly, in the case of the α -glucosidase enzyme, **5d** engages in a hydrogen bond interaction with Arg52.

Additionally, the hydrophobic moiety of **5d**, which includes the indolin-2-one group, participates in π - π interactions with two essential amino acid residues, Phe601 and Trp329. These π - π interactions contribute to the stabilization of **5d** within the active site of the α -glucosidase enzyme and reinforce its inhibitory potential (Fig. 6B). The specific binding interactions observed between **5d** and both α -amylase and α -glucosidase enzymes play a pivotal role in its promising inhibitory effects. By forming these favorable interactions, **5d** effectively interferes with the enzymatic activities of both enzymes, inhibiting their functions, and potentially regulating carbohydrate metabolism, which is highly relevant in the context of developing anti-diabetic drugs.

2.6. MD simulation

The MD simulations allowed for the investigation of the dynamic behavior and structural changes of the system over time. Hence the best docked pose of representative compound **5d** in complex with α -amylase (2QV4) and α -glucosidase (3W37) was subjected to MD simulations for 100 ns. The parameters explored for analysis, such as RMSD, RMSF, RGyr, and inter-molecular hydrogen bonding (H-bonding), were obtained through molecular dynamics (MD) simulations. The RMSD is a critical measure used to assess the structural stability of protein-ligand complexes over time. The positions of the atoms in the protein-ligand complexes were repeatedly recorded as they produced over time throughout the MD simulations. The RMSD was then determined by comparing each time step's atomic locations to the original reference structure. For the **5d**-2QV4 complex, the RMSD values indicate that the structural deviations remained within the range of 1.044 Å to 2.198 Å, with an average of 1.82 Å. These values suggest that the complex exhibited relatively minor fluctuations in its atomic positions during the simulation, well within the commonly accepted limit of 3 Å for RMSD. Similarly, for the **5d**-3W37 complex, the RMSD values ranged from 2.06 Å to 2.47 Å, with an average RMSD of 2.06 Å (Fig. 7A). These values indicate that the complex experienced moderate structural fluctuations throughout the simulation. Despite a minor drift being noted,

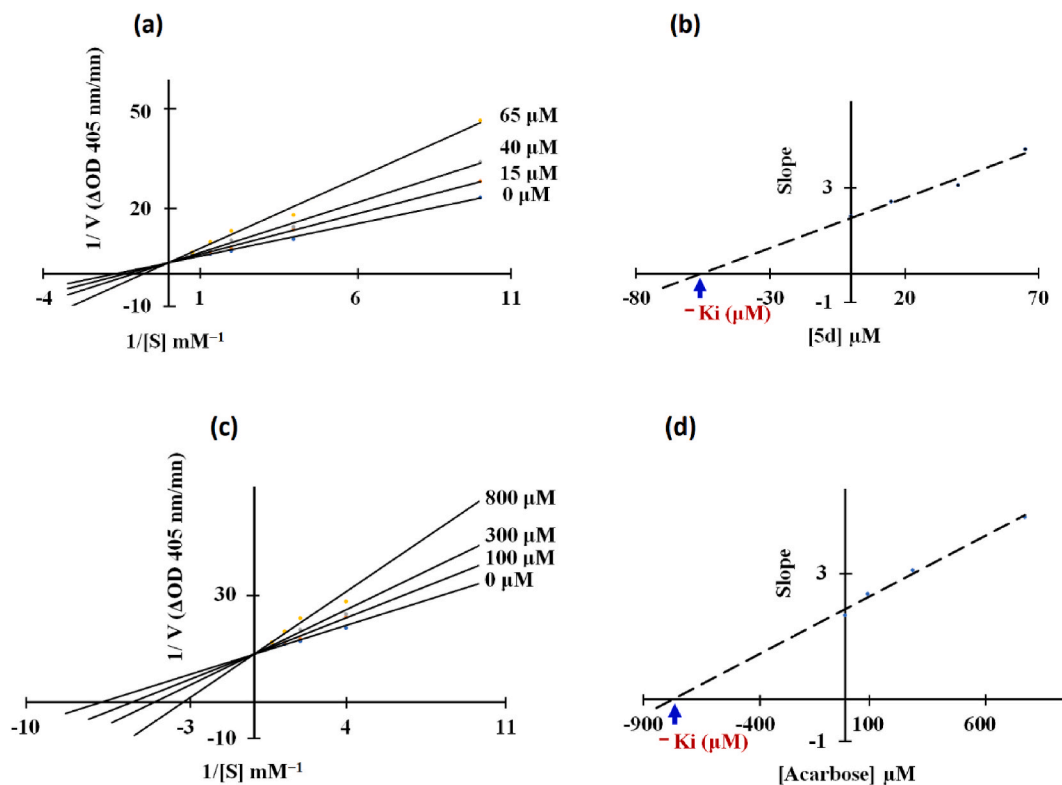
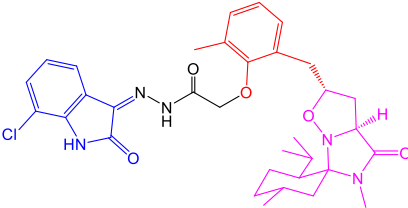
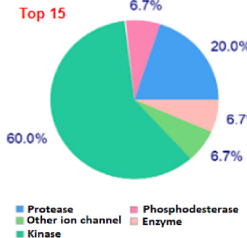
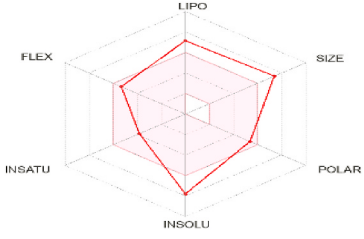
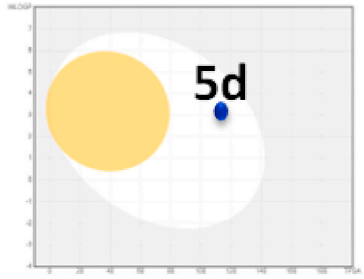


Fig. 5. (a) and (c) Lineweaver–Burk plot of the kinetics of α -glucosidase inhibition by **5d** and acarbose, respectively. (b) and (d) Secondary re-plot of Lineweaver–Burk plots between the slopes of each line on Lineweaver–Burk plot versus various concentrations of **5d** and acarbose, respectively.

this drift remained consistent across the entire duration of the simulation. Significantly, no substantial disparities were detected in the simulation trajectory of the α -amylase (2QV4) and α -glucosidase (3W37) proteins in complexes with **5d**. This observation indicates that the compound **5d** had a relatively stable influence on the behavior of these proteins throughout the simulation, suggesting a potential consistent interaction and impact. The Root Mean Square Fluctuation (RMSF) analysis is a valuable tool used to assess the conformational flexibility of a protein structure during molecular dynamics simulations. It determines the deviation of individual atoms or residues from their original positions in the three-dimensional structure of the macromolecule. Flexible regions with higher RMSF values typically correspond to loops, turns, or certain segments of secondary structures (such as alpha-helices and beta-sheets) that can undergo conformational changes to accommodate ligand binding. Subheadings The graph illustrates that the **5d**-3W37 complex exhibits higher fluctuations than the **5d**-2QV4 complex. In the case of the **5d**-2QV4 complex, specific amino acids demonstrate increased fluctuations, notably Asp236 (2.03 Å), Leu237 (2.08 Å), Gly351 (2.10 Å), Asn350 (2.25 Å), Asn459 (2.62 Å), and Gly460 (2.68 Å), displaying more pronounced variability compared to other residues within the complex (Fig. 7B). Conversely, for the **5d**-3W37 complex, major fluctuations are observed in Phe908 (3.08 Å) and Glu909 (3.29 Å) amino acids (Fig. 7C). Such RMSF fluctuations at the level of individual residues are anticipated due to the absence of any interactions in MD simulation with those specific protein segments. For the **5d**-2QV4 complex, the average RMSF value is calculated to be 0.80 Å. This suggests that, on average, the individual residues within the complex experience relatively minor fluctuations from their original positions throughout the simulation. Such low RMSF values point to a stable conformational behavior, indicating that the complex remains relatively intact and consistent over the simulation duration. In contrast, the **5d**-3W37 complex exhibits a slightly higher average RMSF value of 1.08 Å. This implies that the residues within this complex have a slightly greater degree of conformational flexibility compared to the **5d**-2QV4 complex. The increased RMSF value suggests that certain regions within the **5d**-3W37 complex are more prone to fluctuations, potentially reflecting dynamic interactions or structural adjustments during the simulation. The simulation outcomes revealed a substantial formation of intermolecular hydrogen bonds between the protein residues and the **5d** compound, indicating a robust interaction. Fig. 7D illustrates the dynamic progression of hydrogen bond formation over time. Interestingly, the **5d**-3W37 complex exhibited a relatively higher number of hydrogen bonds (average hydrogen bond number 1.5) compared to the **5d**-2QV4 complex (average hydrogen bond number 1.4). It's noteworthy that these hydrogen bonds remained consistently intact throughout the entire simulation duration for the **5d** compound. This enduring stability underscores the potent binding between **5d** and both α -amylase and α -glucosidase, resulting in an exceptionally steady conformation.

Table 2
ADMET property parameters of **5d**.

Physicochemical Properties		Pharmacokinetics	
Molecular weight	622.15 g/mol	GI absorption	High
Num. heavy atoms	44	BBB permeant	No
Num. arom. heavy atoms	12	P-gp substrate	Yes
Fraction Csp3	0.52	CYP1A2 inhibitor	No
Num. rotatable bonds	8	CYP2C19 inhibitor	No
Num. H-bond acceptors	7	CYP2C9 inhibitor	No
Num. H-bond donors	2	CYP2D6 inhibitor	No
Molar Refractivity	179.70	CYP3A4 inhibitor	Yes
TPSA (Å ²)	112.57	Log Kp (cm/s)	-5.11
Lipophilicity		Druglikeness	
Log Po/w (iLOGP)	4.60	Lipinski	Yes
Log Po/w (XLOGP3)	7.02	Ghose	No
Log Po/w (WLOGP)	3.34	Veber	Yes
Log Po/w (MLOGP)	3.11	Egan	Yes
Log Po/w (SILICOS-IT)	4.56	Muegge	No
Consensus Log Po/w	4.53	Bioavailability Score	0.55
Structure of 5d			
	Target prediction Top 15 		
	Radar plot 		
	Boiled-Egg 		
Toxicity risks			
AMES toxicity (pkCSM)	No	Skin Sensitization (pkCSM)	No
hERG I inhibitor (pkCSM)	No	Carcinogen to rat (PreADMET)	No
hERG II inhibitor (pkCSM)	No	Carcinogen to mouse (PreADMET)	No

3. Materials and methods

3.1. Chemistry

To a solution of hydrazide **4** (or **8**) in ethanol, 1.5 eq. of the appropriate isatin derivative were added in the presence of a little amount of AcOH. The mixture was stirred at reflux in ethanol for 2 h. A TLC control shows the total disappearance of the hydrazide and the formation of a new more polar product. The solvent was evaporated under reduced pressure and the residue was chromatographed on silica gel. The final products **5a-h** were obtained in the form of a brown oily liquid.

N'-((Z)-7-chloro-2-oxoindolin-3-ylidene)-2-(4-(((1S,2S,2'R,3a'S,5R)-2-isopropyl-5,5'-dimethyl-4'-oxotetrahydro-2'H-spiro[cyclohexane-1,6'-imidazo [1,5-b]isoxazol]-2'-yl)methyl)-2-methoxyphenoxy)acetohydrazide (**5a**)

Table 3Glide docking score (in Kcal/mol unit) of **5a-h** in the active sites of anti-diabetic protein receptors of α -amylase and α -glucosidase enzymes.

Name of compounds	α -amylase enzyme (PDB code: 2QV4)	α -glucosidase enzyme (PDB code: 3W37)
5a	-4.969	-4.074
5b	-4.843	-3.843
5c	-5.205	-4.581
5d	-6.602	-5.414
5e	-4.961	-4.319
5f	-5.741	-5.102
5g	-5.507	-3.871
5h	-6.262	-5.381

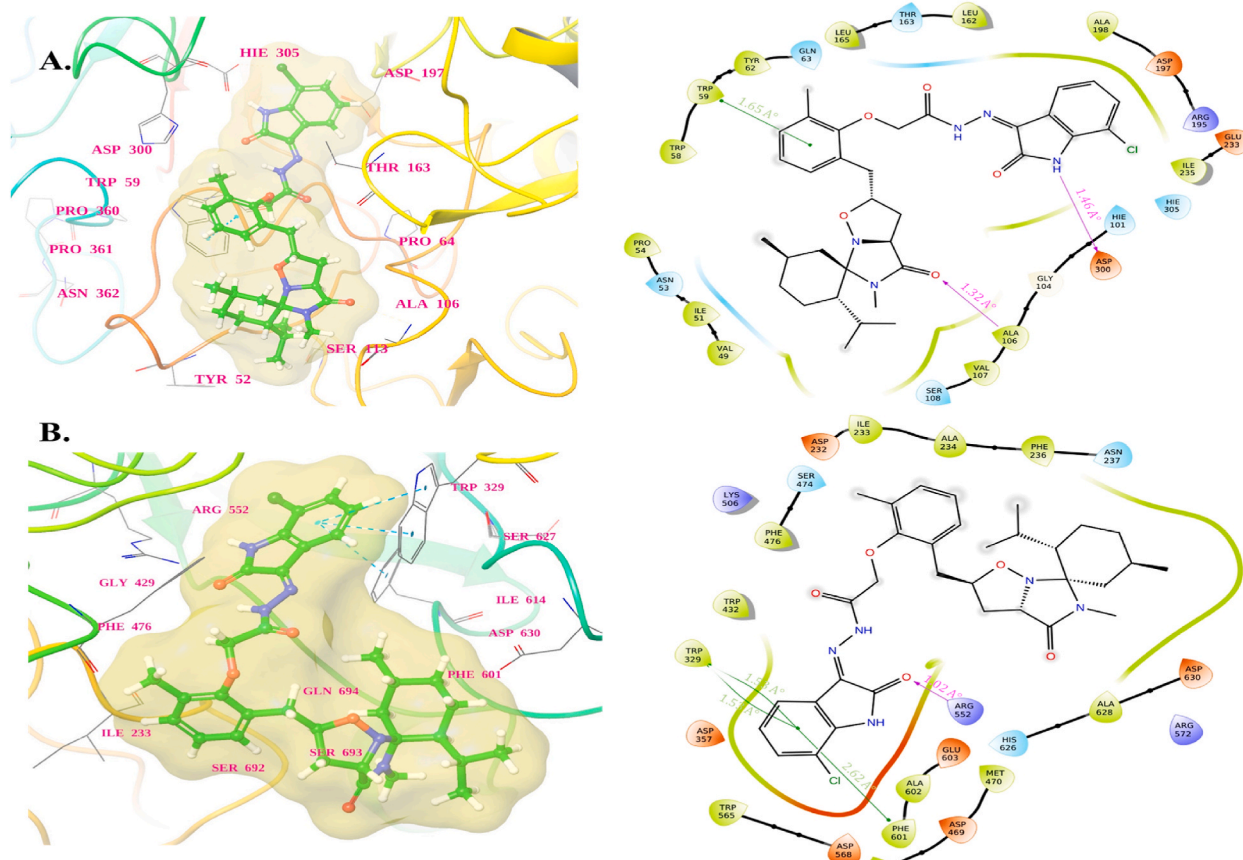


Fig. 6. 2D and 3D Binding poses of representative compound **5d** in the active of site A. α -amylase enzyme (PDB code: 2QV4) and B. α -glucosidase enzyme (PDB code: 3W37) (Hydrogen bond interaction is shown by pink arrow line). (For interpretation of the references to colour in this figure legend, the reader is referred to the Web version of this article.)

IR (FTIR, cm^{-1}): $\nu = 1703$ (amide C=O); 1504 (N–H bonding); 3199 (N–H stretching); 1134 (C–O stretching); 1234 (C–O stretching); 2840 (C–H stretching (aliphatic)); 2939 (C–H stretching (aromatic)). $^1\text{H NMR}$ (400 MHz, CDCl_3) 0.72 (d, 3H, $J = 6.4$ Hz, CH_3); 0.83 (d, 3H, $J = 6.4$ Hz, CH_3); 0.84 (d, 3H, $J = 6.4$ Hz, CH_3); 0.85–0.92 (m, 1H); 1.13 (t, 1H, $J = 12.4$ Hz); 1.30 (dd, 1H, $J = 2.4$ and 12.0 Hz); 1.57–1.71 (m, 3H); 1.76–1.83 (m, 2H); 1.93–1.95 (m, 1H); 2.19 (q, 1H, $J = 10.4$ Hz); 2.64–2.69 (m, 1H); 2.69 (s, 3H, NCH_3); 2.75 (dd, 1H, $J = 4.0$ and 13.6 Hz); 2.82 (dd, 1H, $J = 8.0$ and 14.0 Hz); 3.78–3.84 (m, 1H); 3.86 (s, 3H, OCH_3); 3.91 (d, 1H, $J = 8.4$ Hz); 4.76 (s, 2H); 6.71 (d, 1H, $J = 8.0$ Hz); 6.76 (brs, 1H); 6.87 (d, 1H, $J = 8.0$ Hz); 7.04 (t, 1H, $J = 8.0$ Hz); 7.31 (d, 1H, $J = 8.0$ Hz); 7.68 (d, 1H, $J = 8.0$ Hz); 8.68 (s, 1H, NH); 13.63 (s, 1H, NH).

$^{13}\text{C NMR}$ (100 MHz, CDCl_3) 18.3; 22.1; 22.2; 24.1; 24.3; 26.0; 26.8; 29.7; 34.5; 38.6; 38.8; 40.3; 48.0; 55.9; 66.3; 78.5; 90.1; 113.4; 115.8; 116.0; 120.5; 120.9; 121.6; 124.1; 131.4; 133.9; 137.7; 138.7; 145.4; 149.8; 161.6; 167.0; 172.8.

Anal. Calcd. for $\text{C}_{33}\text{H}_{40}\text{ClN}_5\text{O}_6$ (638.16): C, 62.11; H, 6.32; N, 10.97, Found: C, 62.57; H, 6.22; N, 11.01.

N' -((Z)-5-fluoro-2-oxoindolin-3-ylidene)-2-(4-(((1S,2S,2'R,3a'S,5R)-2-isopropyl-5,5'-dimethyl-4'-oxotetrahydro-2'H-spiro[cyclohexane-1,6'-imidazo [1,5-b]isoxazol]-2'-yl)methyl)-2-methoxyphenoxy)acetohydrazide (**5b**)

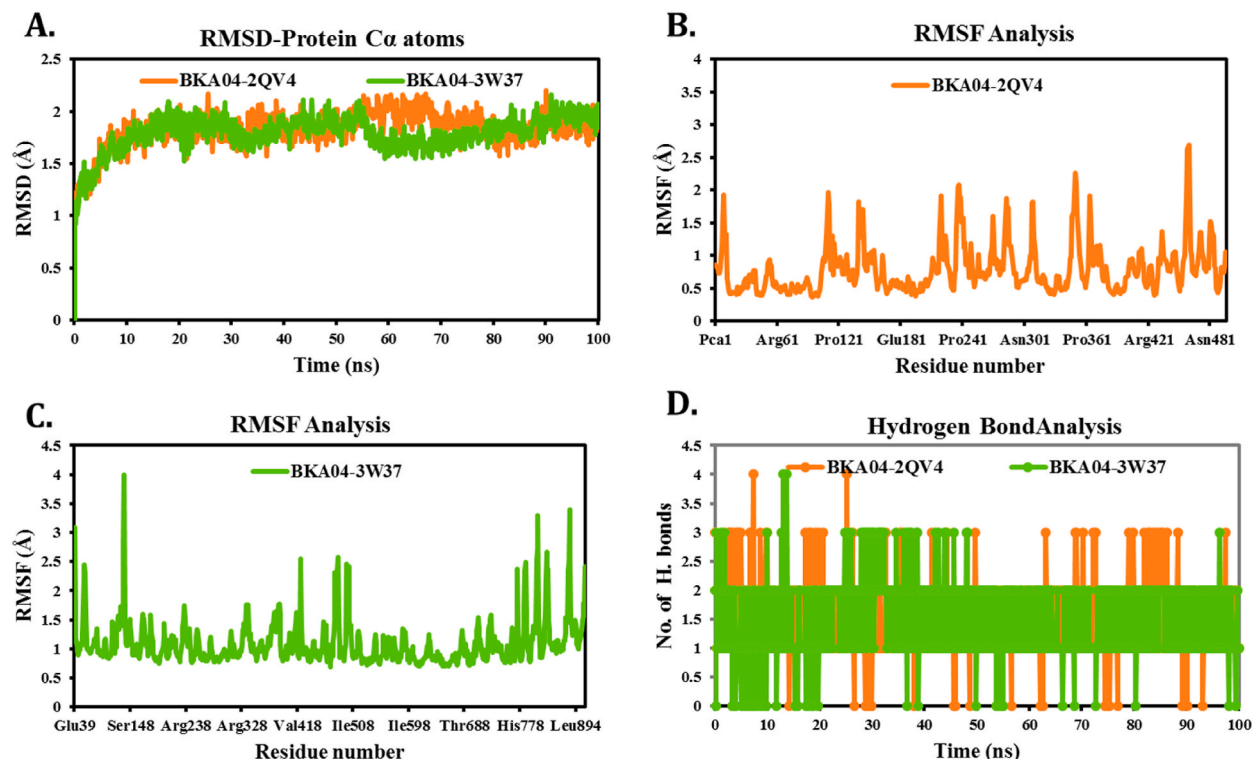


Fig. 7. A. Time-dependent RMSD of C α atoms of **5d**-2QV4 and **5d**-3W37 complexes; B. RMSF of individual amino acids of C α atoms of **5d**-2QV4 complex; C. RMSF of individual amino acids of C α atoms of **5d**-3W37 complex; D. Time-dependent Hydrogen bond analysis of **5d**-2QV4 and **5d**-3W37 complexes.

IR (FTIR, cm^{-1}): $\nu = 1699$ (amide C=O); 1595 (N–H bonding); 3220 (N–H stretching); 1175 (C–O stretching); 1201 (C–O stretching); 2868 (C–H stretching (aliphatic)); 2951 (C–H stretching (aromatic)). ¹H NMR (400 MHz, CDCl_3) 0.72 (d, 3H, $J = 6.4$ Hz, CH_3); 0.83 (d, 3H, $J = 6.4$ Hz, CH_3); 0.84 (d, 3H, $J = 6.4$ Hz, CH_3); 0.85–0.92 (m, 1H); 1.14 (t, 1H, $J = 12$ Hz); 1.30 (dd, 1H, $J = 2.4$ and 12.0 Hz); 1.59 (dd, 1H, $J = 2.8$ and 12.8 Hz); 1.64–1.79 (m, 3H); 1.93–1.97 (m, 1H); 2.19 (q, 1H, $J = 10.8$ Hz); 2.64 (dd, 1H, $J = 3.6$ and 12 Hz); 2.69 (s, 3H, NCH_3); 2.75–2.86 (m, 2H); 3.79–3.81 (m, 1H); 3.84 (s, 3H, OCH_3); 3.99 (d, 1H, $J = 8.4$ Hz); 4.77 (s, 2H); 6.70 (d, 1H, $J = 8.4$ Hz); 6.76 (brs, 1H); 6.81 (dd, 1H, $J = 4.0$ and 8.0 Hz); 6.86 (d, 1H, $J = 8.0$ Hz); 6.99 (dt, 1H, $J = 1.5$ and 8.8 Hz); 7.45 (d, 1H, $J = 6.0$ Hz); 9.16 (s, 1H, NH); 13.70 (s, 1H, NH).

¹³C NMR (100 MHz, CDCl_3) 18.3; 22.1; 22.2; 24.1; 24.3; 26.0; 26.8; 29.7; 34.4; 38.5; 40.3; 48.0; 56.0; 66.4; 78.5; 90.1; 109.4; 109.7; 111.7; 111.8; 113.5; 115.8; 118.3; 118.5; 121.0; 133.7; 137.7; 138.4; 145.4; 149.8; 162.6; 167.1; 172.9.

Anal. Calcd. for $\text{C}_{33}\text{H}_{40}\text{FN}_5\text{O}_6$ (621.71): C, 63.75; H, 6.49; N, 11.26, Found: C, 63.47; H, 6.55; N, 10.98.

N'-((Z)-6-bromo-2-oxoindolin-3-ylidene)-2-(4-(((1S,2S,2'R,3a'S,5R)-2-isopropyl-5,5'-dimethyl-4'-oxotetrahydro-2'H-spiro[cyclohexane-1,6'-imidazo [1,5-b]isoxazol-2'-yl)methyl]-2-methoxyphenoxy)acetohydrazide (**5c**)

IR (FTIR, cm^{-1}): $\nu = 1701$ (amide C=O); 1508 (N–H bonding); 3236 (N–H stretching); 1150 (C–O stretching); 1203 (C–O stretching); 2862 (C–H stretching (aliphatic)); 2947 (C–H stretching (aromatic)). ¹H NMR (400 MHz, CDCl_3) 0.74 (d, 3H, $J = 6.4$ Hz, CH_3); 0.83 (d, 3H, $J = 6.4$ Hz, CH_3); 0.84 (d, 3H, $J = 6.4$ Hz, CH_3); 0.85–0.92 (m, 1H); 1.14 (t, 1H, $J = 12$ Hz); 1.31 (dd, 1H, $J = 2.0$ and 12.0 Hz); 1.61 (dd, 1H, $J = 2.8$ and 12.8 Hz); 1.65–1.79 (m, 3H); 1.94 (m, 1H); 2.19 (q, 1H, $J = 10.8$ Hz); 2.64 (dd, 1H, $J = 3.6$ and 12 Hz); 2.69 (s, 3H, NCH_3); 2.76 (dd, 1H, $J = 4.4$ and 12 Hz); 2.84 (dd, 1H, $J = 8$ and 13.6 Hz); 3.74–3.81 (m, 1H); 3.85 (s, 3H, OCH_3); 3.99 (d, 1H, $J = 8.8$ Hz); 4.77 (s, 2H); 6.70 (dd, 1H, $J = 1.6$ and 8.4 Hz); 6.76 (brs, 1H); 6.85 (d, 1H, $J = 8.4$ Hz); 7.06 (brs, 1H); 7.19 (d, 1H, $J = 8.0$ Hz); 7.59 (d, 1H, $J = 8.4$ Hz); (dt, 1H, $J = 1.5$ and 8.8 Hz); 9.38 (s, 1H, NH); 13.64 (s, 1H, NH).

¹³C NMR (100 MHz, CDCl_3) 18.3; 22.1; 22.2; 24.1; 24.3; 26.1; 26.8; 29.7; 34.4; 38.5; 38.7; 40.3; 48.0; 56.0; 66.3; 78.5; 90.2; 113.6; 114.4; 115.6; 118.9; 121.0; 123.4; 125.8; 126.3; 133.6; 138.0; 142.7; 145.4; 149.8; 162.3; 167.1; 172.9.

Anal. Calcd. for $\text{C}_{33}\text{H}_{40}\text{BrN}_5\text{O}_6$ (682.62): C, 58.07; H, 5.91; N, 10.26, Found: C, 57.88; H, 5.85; N, 10.33.

N'-((Z)-7-chloro-2-oxoindolin-3-ylidene)-2-(2-(((1S,2S,2'R,3a'S,5R)-2-isopropyl-5,5'-dimethyl-4'-oxotetrahydro-2'H-spiro[cyclohexane-1,6'-imidazo [1,5-b]isoxazol-2'-yl)methyl]-6-methylphenoxy)acetohydrazide (**5d**)

IR (FTIR, cm^{-1}): $\nu = 1697$ (amide C=O); 1506 (N–H bonding); 3294 (N–H stretching); 1126 (C–O stretching); 1215 (C–O stretching); 2862 (C–H stretching (aliphatic)); 2943 (C–H stretching (aromatic)). ¹H NMR (400 MHz, CDCl_3) 0.49 (d, 3H, $J = 6.4$ Hz, CH_3); 0.76 (d, 3H, $J = 7.2$ Hz, CH_3); 0.78 (d, 3H, $J = 7.2$ Hz, CH_3); 0.74–0.78 (m, 1H); 1.00 (t, 1H, $J = 12.4$ Hz); 1.22–1.30 (m, 2H); 1.52–1.61 (m, 3H); 1.68 (d, 1H, $J = 13.2$ Hz); 1.76–1.81 (m, 1H); 2.07 (q, 1H, $J = 10.8$ Hz); 2.24 (s, 3H, CH_3); 2.48 (ddd, 2H, $J = 3.2$, 5.6 and 12.0 Hz); 2.65 (s, 3H, NCH_3); 3.00 (d, 1H, $J = 12$ Hz); 3.92 (d, 1H, $J = 8.8$ Hz); 4.04 (t, 1H, $J = 8.4$ Hz); 4.28 (d, 1H, $J = 15.2$

Hz); 4.67 (d, 1H, $J = 15.6$ Hz); 6.80 (dd, 1H, $J = 4.0$ and 8.4 Hz); 6.90–6.96 (m, 2H); 7.00 (d, 1H, $J = 6.8$ Hz); 7.11 (d, 1H, $J = 6.8$ Hz); 7.45 (dd, 1H, $J = 2.0$ and 7.6 Hz); 9.27 (s, 1H, NH); 14.17 (s, 1H, NH).

^{13}C NMR (100 MHz, CDCl_3) 18.3; 20.9; 22.1; 22.2; 24.1; 24.3; 26.1; 29.7; 34.4; 38.6; 38.8; 40.3; 48.0; 66.4; 69.1; 78.5; 90.1; 110.5; 113.5; 115.4; 120.1; 121.0; 122.9; 132.4; 133.0; 133.5; 138.8; 139.2; 145.5; 149.8; 162.3; 166.9; 172.9.

Anal. Calcd. for $\text{C}_{33}\text{H}_{40}\text{ClN}_5\text{O}_5$ (622.16): C, 63.71; H, 6.48; N, 11.26, Found: C, 63.88; H, 6.44; N, 11.22.

N' -(Z)-6-bromo-2-oxoindolin-3-ylidene)-2-(2-(((1S,2S,2'R,3a'S,5R)-2-isopropyl-5,5'-dimethyl-4'-oxotetrahydro-2'H-spiro[cyclohexane-1,6'-imidazo [1,5-b]isoxazol]-2'-yl)methyl)-6-methylphenoxy)acetohydrazide (**5e**)

IR (FTIR, cm^{-1}): $\nu = 1695$ (amide $\text{C}=\text{O}$); 1440 (N–H bonding); 3207 (N–H stretching); 1145 (C–O stretching); 1215 (C–O stretching); 2866 (C–H stretching (aliphatic)); 2953 (C–H stretching (aromatic)). ^1H NMR (400 MHz, CDCl_3) 0.52 (d, 3H, $J = 6.4$ Hz, CH_3); 0.82 (d, 3H, $J = 7.2$ Hz, CH_3); 0.84 (d, 3H, $J = 7.2$ Hz, CH_3); 0.85–0.91 (m, 1H); 1.06 (t, 1H, $J = 12.4$ Hz); 1.25–1.29 (m, 2H) 1.56–1.59 (m, 2H); 1.67 (d, 1H, $J = 12.8$ Hz); 1.74 (d, 1H, $J = 15.2$ Hz); 1.81–1.83 (m, 1H); 2.12 (q, 1H, $J = 11.6$ Hz); 2.32 (s, 3H, CH_3); 2.54 (ddd, 1H, $J = 3.6, 6.8$ and 13.6 Hz); 2.73 (s, 3H, NCH_3); 2.77 (dd, 1H, $J = 4.8$ and 12.4 Hz); 3.07 (d, 1H, $J = 12$ Hz); 4.0 (d, 1H, $J = 8.8$ Hz); 4.15 (t, 1H, $J = 6.0$ Hz); 4.32 (d, 1H, $J = 15.6$ Hz); 4.76 (d, 1H, $J = 15.6$ Hz); 6.99 (t, 1H, $J = 7.2$ Hz); 7.05–7.06 (m, 2H); 7.18 (d, 1H, $J = 7.2$ Hz); 7.35 (d, 1H, $J = 7.6$ Hz); 7.73 (d, 1H, $J = 7.2$ Hz); 9.41 (s, 1H, NH); 14.25 (s, 1H, NH).

^{13}C NMR (100 MHz, CDCl_3) 16.6; 18.3; 22.0; 22.2; 24.2; 24.3; 26.2; 29.7; 32.7; 34.5; 39.0; 39.9; 48.2; 66.7; 70.7; 77.8; 90.4; 116.5; 120.6; 121.4; 124.1; 124.9; 129.8; 130.2; 130.5; 131.1; 131.6; 139.0; 139.3; 153.1; 162.4; 166.3; 173.0.

Anal. Calcd. for $\text{C}_{33}\text{H}_{40}\text{BrN}_5\text{O}_5$ (666.62): C, 59.46; H, 6.05; N, 10.51, Found: C, 59.18; H, 6.08; N, 10.63.

N' -(Z)-5-fluoro-2-oxoindolin-3-ylidene)-2-(2-(((1S,2S,2'R,3a'S,5R)-2-isopropyl-5,5'-dimethyl-4'-oxotetrahydro-2'H-spiro[cyclohexane-1,6'-imidazo [1,5-b]isoxazol]-2'-yl)methyl)-6-methylphenoxy)acetohydrazide (**5f**)

IR (FTIR, cm^{-1}): $\nu = 1697$ (amide $\text{C}=\text{O}$); 1490 (N–H bonding); 3207 (N–H stretching); 1149 (C–O stretching); 1203 (C–O stretching); 2866 (C–H stretching (aliphatic)); 2951 (C–H stretching (aromatic)). ^1H NMR (400 MHz, CDCl_3) 0.55 (d, 3H, $J = 6.4$ Hz, CH_3); 0.81 (d, 3H, $J = 7.2$ Hz, CH_3); 0.83 (d, 3H, $J = 7.2$ Hz, CH_3); 0.82–0.85 (m, 1H); 1.06 (t, 1H, $J = 12.4$ Hz); 1.28–1.35 (m, 2H); 1.58–1.67 (m, 3H); 1.72–1.87 (m, 2H); 2.14 (q, 1H, $J = 10.8$ Hz); 2.30 (s, 3H, CH_3); 2.50–2.67 (m, 2H); 2.71 (s, 3H, NCH_3); 3.06 (d, 1H, $J = 12$ Hz); 3.98 (d, 1H, $J = 8.8$ Hz); 4.11 (t, 1H, $J = 8.4$ Hz); 4.34 (d, 1H, $J = 15.2$ Hz); 4.73 (d, 1H, $J = 15.6$ Hz); 6.86 (dd, 1H, $J = 4.0$ and 8.4 Hz); 7.00–7.02 (m, 2H); 7.06 (d, 1H, $J = 6.8$ Hz); 7.16 (d, 1H, $J = 6.8$ Hz); 7.50 (dd, 1H, $J = 2.0$ and 7.6 Hz); 9.33 (s, 1H, NH); 14.23 (s, 1H, NH)

^{13}C NMR (100 MHz, CDCl_3) 16.5; 18.3; 21.9; 22.2; 24.1; 24.4; 26.2; 29.6; 32.7; 34.4; 38.9; 39.9; 48.2; 66.6; 70.7; 77.7; 90.4; 109.8; 112.1; 118.7; 121.1; 124.9; 129.6; 130.2; 130.6; 131.0; 137.9; 139.11; 139.15; 153.2; 163.1; 166.3; 173.1.

Anal. Calcd. for $\text{C}_{33}\text{H}_{40}\text{FN}_5\text{O}_5$ (605.71): C, 65.44; H, 6.66; N, 11.56, Found: C, 65.23; H, 6.58; N, 11.52.

2-(2-(((1S,2S,2'R,3a'S,5R)-2-isopropyl-5,5'-dimethyl-4'-oxotetrahydro-2'H-spiro[cyclohexane-1,6'-imidazo [1,5-b]isoxazol]-2'-yl)methyl)-6-methylphenoxy)- N' -(Z)-5-methyl-2-oxoindolin-3-ylidene)acetohydrazide (**5g**)

IR (FTIR, cm^{-1}): $\nu = 1699$ (amide $\text{C}=\text{O}$); 1471 (N–H bonding); 3224 (N–H stretching); 1122 (C–O stretching); 1199 (C–O stretching); 2868 (C–H stretching (aliphatic)); 2941 (C–H stretching (aromatic)). ^1H NMR (400 MHz, CDCl_3) 0.55 (d, 3H, $J = 6.4$ Hz, CH_3); 0.81 (d, 3H, $J = 6.8$ Hz, CH_3); 0.83 (d, 3H, $J = 7.2$ Hz, CH_3); 0.82–0.84 (m, 1H); 1.05 (t, 1H, $J = 12.4$ Hz); 1.24–1.36 (m, 2H); 1.54–1.68 (m, 3H); 1.72–1.84 (m, 2H); 2.13 (q, 1H, $J = 10.8$ Hz); 2.30 (s, 6H, 2CH_3); 2.52–2.66 (m, 2H); 2.70 (s, 3H, NCH_3); 3.06 (d, 1H, $J = 13.2$ Hz); 3.97 (d, 1H, $J = 8.0$ Hz); 4.08–4.13 (m, 1H); 4.34 (d, 1H, $J = 15.6$ Hz); 4.71 (d, 1H, $J = 15.6$ Hz); 6.78 (d, 1H, $J = 7.6$ Hz); 6.99 (d, 1H, $J = 7.6$ Hz); 7.05 (d, 1H, $J = 7.2$ Hz); 7.10 (d, 1H, $J = 8.0$ Hz); 7.15 (d, 1H, $J = 7.6$ Hz); 7.60 (brs, 1H); 9.19 (s, 1H, NH); 14.20 (s, 1H, NH).

^{13}C NMR (100 MHz, CDCl_3) 16.5; 18.3; 20.9; 21.9; 22.2; 24.1; 24.3; 26.2; 29.6; 32.7; 34.4; 38.9; 39.9; 48.1; 66.6; 70.8; 77.7; 90.3; 110.9; 119.8; 122.8; 124.8; 129.5; 130.1; 130.6; 131.1; 132.6; 132.8; 139.7; 139.8; 153.3; 163.1; 166.2; 173.0.

Anal. Calcd. for $\text{C}_{34}\text{H}_{43}\text{N}_5\text{O}_5$ (601.75): C, 67.86; H, 7.20; N, 11.64, Found: C, 67.53; H, 7.13; N, 11.57.

N' -(Z)-7-fluoro-2-oxoindolin-3-ylidene)-2-(2-(((1S,2S,2'R,3a'S,5R)-2-isopropyl-5,5'-dimethyl-4'-oxotetrahydro-2'H-spiro[cyclohexane-1,6'-imidazo [1,5-b]isoxazol]-2'-yl)methyl)-6-methylphenoxy)acetohydrazide (**5h**)

IR (FTIR, cm^{-1}): $\nu = 1703$ (amide $\text{C}=\text{O}$); 1481 (N–H bonding); 3464 (N–H stretching); 1122 (C–O stretching); 1200 (C–O stretching); 2870 (C–H stretching (aliphatic)); 2953 (C–H stretching (aromatic)). ^1H NMR (400 MHz, CDCl_3) 0.49 (d, 3H, $J = 6.4$ Hz, CH_3); 0.76 (d, 3H, $J = 7.2$ Hz, CH_3); 0.78 (d, 3H, $J = 7.2$ Hz, CH_3); 0.75–0.78 (m, 1H); 1.00 (t, 1H, $J = 12.4$ Hz); 1.26–1.29 (m, 2H); 1.52–1.61 (m, 3H); 1.68 (d, 1H, $J = 13.2$ Hz); 1.76–1.81 (m, 1H); 2.07 (q, 1H, $J = 10.8$ Hz); 2.24 (s, 3H, CH_3); 2.48 (ddd, 2H, $J = 3.2, 5.6$ and 12.0 Hz); 2.65 (s, 3H, NCH_3); 3.00 (d, 1H, $J = 12$ Hz); 3.92 (d, 1H, $J = 8.8$ Hz); 4.04 (t, 1H, $J = 8.4$ Hz); 4.28 (d, 1H, $J = 15.2$ Hz); 4.67 (d, 1H, $J = 15.6$ Hz); 6.80 (dd, 1H, $J = 4.0$ and 8.4 Hz); 6.90–6.96 (m, 2H); 7.00 (d, 1H, $J = 6.8$ Hz); 7.11 (d, 1H, $J = 6.8$ Hz); 7.45 (dd, 1H, $J = 2.0$ and 7.6 Hz); 9.27 (s, 1H, NH); 14.17 (s, 1H, NH).

^{13}C NMR (100 MHz, CDCl_3) 16.5; 18.3; 21.9; 22.2; 24.1; 24.4; 26.2; 29.6; 32.7; 34.4; 38.9; 39.9; 48.2; 66.6; 70.7; 77.7; 90.4; 109.8; 112.1; 118.7; 121.1; 124.9; 129.6; 130.2; 130.6; 131.0; 137.9; 139.11; 139.15; 153.2; 163.1; 166.3; 173.1.

^{13}C NMR (100 MHz, CDCl_3) 18.3; 20.9; 22.1; 22.2; 24.1; 24.3; 26.1; 29.7; 34.4; 38.6; 38.8; 40.3; 48.0; 56.0; 66.4; 78.5; 90.1; 110.5; 113.5; 115.4; 120.1; 121.0; 122.9; 132.4; 133.0; 133.5; 138.8; 139.2; 145.5; 149.8; 162.3; 166.9; 172.9.

Anal. Calcd. for $\text{C}_{33}\text{H}_{40}\text{FN}_5\text{O}_5$ (605.71): C, 65.44; H, 6.66; N, 11.56, Found: C, 65.32; H, 6.58; N, 11.54.

3.2. α -Amylase and α -glucosidase inhibition assays

The antidiabetic activity of the synthesized compounds towards human pancreatic α -amylase and human lysosomal acid- α -glucosidase enzymes was investigated using the same experimental method as done previously with slight modification [33].

Acarbose was used as standard. The percent of inhibition for both enzymes was calculated via the following formula:

$$\% \text{ inhibition} = \frac{\text{Abs}(\text{blank}) - \text{Abs}(\text{test compound})}{\text{Abs}(\text{blank})} \times 100$$

The results were expressed as IC₅₀ (μM) and all the experiments were carried out in triplicates.

3.3. Enzymes kinetic study

kinetic studies were carried out based on the above IC₅₀ values and the in vitro assays for the most potent inhibitor (**5d**) and acarbose to determine their inhibition mode towards both enzymes. A volume of 20 μL was incubated for 15 min at 30 °C by using the varying concentration of the inhibitor **5d** against α-amylase (0, 5, 15 and 33 μM) and α-glucosidase (0, 15, 40, and 65 mM) with varying concentrations of inhibitor substrate (starch) in the range 0.25–5 mM, whereas the concentrations for the inhibitor substrate (*p*-nitrophenyl-α-D-glucopyranoside, *P*-NPG) were in the range 0.1–1.3 mM, respectively, according to some previously methods, with minor modification [83,84]. The type of inhibition of the enzyme was assessed by preparing Lineweaver-Burk plots of the inverse of the velocities (1/*V*) versus the inverse of the substrate's concentration 1/[*S*] mM⁻¹, and change in absorbance was measured spectrophotometrically at 405 nm. The constant of inhibition, *K_i*, was determined by the secondary plot of the slope versus the inhibitor concentration.

3.4. Molecular docking and molecular dynamic (MD) simulation studies

A molecular docking study was conducted to better understand the molecular basis of the interaction of newly synthesized derivative with anti-diabetic protein receptors. The crystalline structures of the α-glucosidase enzyme (identified by the PDB code: 3W37) and the α-amylase enzyme (identified by the PDB code: 2QV4) were obtained from the protein data bank. Molecular docking was performed using Schrödinger glide, and MD simulation was performed using Schrödinger's Desmond program. The same technique as described in our earlier article for Molecular docking and MD simulation methods is used here [85].

3.5. ADMET property predictions

The ADMET prediction was studied using the following online servers, <http://www.swissadme.ch/>, and <https://preadmet.webservice.bmdrc.org/>, accessed on 4/11/2023 [86,87]. For prediction of pharmacokinetic properties we have used web server <https://biosig.lab.uq.edu.au/pkcsim/> accessed on 4/11/2023 [88].

3.6. Statistical analysis

SPSS 19 (SPSS Ltd., Woking, United Kingdom) was used for the statistical analysis of the resulting experimental data. The Tukey test was used for the comparison of averages. The P-value <0.05 was used to show the statistical significance of the results.

4. Conclusions

In the present work, we designed and synthesized a new series of isoxazolidine-isatin hybrids. These compounds exhibited varying and interesting enzymatic inhibitory potential against α-amylase and α-glucosidase. Among the synthesized compounds, **5d** exhibited impressive α-amylase and α-glucosidase inhibitory activity with IC₅₀ values of 30.39 ± 1.52 μM and 65.1 ± 3.11 μM, respectively. Enzyme kinetic analysis showed that **5d** was the most active compound as well as acarbose, perfectly competed with the substrate to attach to the active site of both enzymes. SAR study revealed the importance of substituent groups on the isatin moiety. The effectiveness of **5d** as promising future drug was examined and justified through computer-aided ADMET calculations. Molecular docking and dynamic simulation against the potent inhibitor **5d** were in accordance with the in vitro results and justify its stabilization inside both enzymes pocket with a dock score of -6.602 kcal/mol (**5d**-2QV4) and -5.414 kcal/mol (**5d**-3W37), leading to the best pharmacophore. Thus, the next objective in this approach will be to explore the in vivo activity of **5d** in animal models and to develop safer as well as efficient oral antidiabetic drug candidates.

CRedit authorship contribution statement

Siwar Ghannay: Writing – review & editing, Writing – original draft, Investigation, Conceptualization. **Budur Saleh Aldhafeeri:** Resources, Methodology, Conceptualization. **Iqrar Ahmad:** Writing – original draft, Software, Formal analysis. **Abuzar E.A.E. Albadri:** Formal analysis, Data curation. **Harun Patel:** Software, Methodology. **Adel Kadri:** Writing – review & editing, Writing – original draft, Validation, Supervision, Methodology, Conceptualization. **Kaïss Aouadi:** Writing – review & editing, Writing – original draft, Visualization, Validation, Supervision, Conceptualization.

Declaration of competing interest

The authors declare that they have no known competing financial interests or personal relationships that could have appeared to influence the work reported in this paper.

Appendix A. Supplementary data

Supplementary data to this article can be found online at <https://doi.org/10.1016/j.heliyon.2024.e25911>.

References

- [1] A.I. Aedh, M.S. Alshahrani, M.A. Huneif, I.F. Pryme, R. Oruch, A Glimpse into Milestones of insulin Resistance and an updated review of its management, *Nutrients* 15 (2023) 921.
- [2] Y. Chen, S. Tan, M. Liu, J. Li, LncRNA TINCR is downregulated in diabetic cardiomyopathy and relates to cardiomyocyte apoptosis, *Scand. Cardiovasc. J.* 52 (2018) 335–339.
- [3] M.A.M. Gad-Elkareem, E.H. Abdelgadir, O.M. Badawy, A. Kadri, Potential antidiabetic effect of ethanolic and aqueous-ethanolic extracts of *Ricinus communis* leaves on streptozotocin-induced diabetes in rats, *PeerJ* 7 (2019) e6441.
- [4] Y.Y. Yang, L.X. Shi, J.H. Li, L.Y. Yao, D.X. Xiang, Piperazine ferulate ameliorates the development of diabetic nephropathy by regulating endothelial nitric oxide synthase, *Mol. Med. Rep.* 19 (2019) 2245–2253.
- [5] J. Chen, X. Li, H. Liu, D. Zhong, K. Yin, Y. Li, L. Zhu, C. Xu, M. Li, C. Wang, Bone marrow stromal cell-derived exosomal circular RNA improves diabetic foot ulcer wound healing by activating the nuclear factor erythroid 2-related factor 2 pathway and inhibiting ferroptosis, *Diabet. Med.* 40 (2023) e15031.
- [6] Z. Gao, X. Pan, J. Shao, X. Jiang, Z. Su, K. Jin, J. Ye, Automatic interpretation and clinical evaluation for fundus fluorescein angiography images of diabetic retinopathy patients by deep learning, *Br. J. Ophthalmol.* 107 (2023) 1852–1858.
- [7] X. Zhao, Y. Zhang, Y. Yang, J. Pan, Diabetes-related avoidable hospitalisations and its relationship with primary healthcare resourcing in China: a cross-sectional study from Sichuan Province, *Health Soc. Care Community* 30 (2022) e1143–e1156.
- [8] B. Waheed, S.M.M. Shah, F. Hussain, M.I. Khan, A. Zeb, M.S. Jan, Synthesis, antioxidant, and antidiabetic activities of Ketone derivatives of Succinimide, *J Evid Based Complementary Altern Med* 2022 (2023). ID 1445604.
- [9] O.M. Alshehri, M.H. Mahnashi, A. Sadiq, R. Zafar, M.S. Jan, F. Ullah, M.A. Alshehri, S. Alshamrani, E.E. Hassan, Succinimide derivatives as antioxidant Anticholinesterases, anti- α -amylase, and anti- α -glucosidase: in vitro and in silico approaches, *J Evid Based Complementary Altern Med* 2022 (2022). ID 6726438.
- [10] M. Shah, M.S. Jan, A. Sadiq, S. Khan, U. Rashid, SAR and lead optimization of (Z)-5-(4-hydroxy-3-methoxybenzylidene)-3-(2-morpholinoacetyl)thiazolidine-2,4-dione as a potential multi-target antidiabetic agent, *Eur. J. Med. Chem.* 258 (2023) 115591.
- [11] Z. Li, M. Zeng, K. Geng, D. Lai, Z. Xu, W. Zhou, Chemical constituents and hypoglycemic mechanisms of *Dendrobium nobile* in treatment of type 2 diabetic rats by UPLC-ESI-Q-Orbitrap, *Network Pharmacology and in vivo experimental verification*, *Molecules* 28 (2023) 2683.
- [12] X. Wang, X. Li, S. Wei, M. Wang, Y. Xu, W. Hu, Z. Gao, R. Liu, S. Wang, G. Ji, Discovery of novel and selective G-protein coupled receptor 120 (GPR120) Agonists for the treatment of type 2 diabetes mellitus, *Molecules* 27 (2022) 9018.
- [13] L. Dilworth, A. Facey, F. Omoruyi, Diabetes mellitus and its metabolic complications: the role of Adipose Tissues, *Int. J. Mol. Sci.* 22 (2021) 7644.
- [14] A. Pervaiz, M.S. Jan, S.M. Hassan Shah, A. Khan, R. Zafar, B. Ansari, M. Shahid, F. Hussain, M. Ijaz Khan, A. Zeb, S.M. Mukarram Shah, Comparative in-vitro anti-inflammatory, anticholinesterase and antidiabetic evaluation: computational and kinetic assessment of succinimides cyano-acetate derivatives, *J. Biomol. Struct. Dyn.* (2022), <https://doi.org/10.1080/07391102.2022.2069862>.
- [15] S. Alam, M.K. Hasan, S. Neaz, N. Hussain, M.F. Hossain, T. Rahman, Diabetes mellitus: Insights from Epidemiology, Biochemistry, risk factors, Diagnosis, complications and comprehensive management, *Diabetology* 2 (2021) 36–50.
- [16] J. Poonosamy, P. Lopes, P. Huret, R. Dardari, A. Penfornis, C. Thomas, D. Dardari, Impact of intensive glycemic treatment on diabetes complications—a systematic review, *Pharmaceutics* 15 (2023) 1791.
- [17] B. Abubakar, D. Usman, K.O. Sanusi, N.H. Azmi, M.U. Imam, Preventive epigenetic mechanisms of functional foods for type 2 diabetes, *Diabetology* 4 (2023) 259–277.
- [18] C. Salom Vendrell, E. García Tercero, J.B. Moro Hernández, B.A. Cedeno-Veloz, Sarcopenia as a little-recognized comorbidity of type II diabetes mellitus: a review of the diagnosis and treatment, *Nutrients* 15 (2023) 4149.
- [19] U. Galicia-Garcia, A. Benito-Vicente, S. Jebari, A. Larrea-Sebal, H. Siddiqi, K.B. Uribe, H. Ostolaza, C. Martín, Pathophysiology of type 2 diabetes mellitus, *Int. J. Mol. Sci.* 21 (2020) 6275.
- [20] K. Zhang, R. Dong, X. Hu, C. Ren, Y. Li, Oat-based foods: chemical constituents, glycemic Index, and the effect of processing, *Foods* 10 (2021) 1304.
- [21] S. Chen, B. Lin, J. Gu, T. Yong, X. Gao, Y. Xie, C. Xiao, J.Y. Zhan, Q. Wu, Binding interaction of Betulinic acid to α -glucosidase and its Alleviation on postprandial hyperglycemia, *Molecules* 27 (2022) 2517.
- [22] R. Vieira, S.B. Souto, E. Sánchez-López, A. López Machado, P. Severino, S. Jose, A. Santini, A. Fortuna, M.L. García, A.M. Silva, et al., Sugar-lowering drugs for type 2 diabetes mellitus and metabolic Syndrome—review of Classical and new compounds: Part-I, *Pharmaceutics* 12 (2019) 152.
- [23] S.H. Adam, I.F. Abu, D.A.M. Kamal, A. Febriza, M.I.A.M. Kashim, M.H. Mokhtar, A review of the potential Health benefits of *Nigella sativa* on Obesity and its associated Complications, *Plants* 12 (2023) 3210.
- [24] N. Djermane, L. Gali, R. Arhab, N. Gherraf, C. Bensouici, R. Erenler, M. Gok, A. Abdessamed, Chemical composition and in vitro evaluation of antioxidant, antimicrobial, and enzyme inhibitory activities of *Erucaria uncata* and *Thymeleae hirsuta*, *Biocatal. Agric. Biotechnol.* 29 (2020) 101834.
- [25] H. Kashtoh, K.-H. Baek, New insights into the Latest advancement in α -amylase inhibitors of plant origin with anti-diabetic effects, *Plants* 12 (2023) 2944.
- [26] H. Kashtoh, K.-H. Baek, Recent updates on Phytoconstituent α -glucosidase inhibitors: an approach towards the treatment of type two diabetes, *Plants* 11 (2022) 2722.
- [27] H.E.P. Abeleda, A.P. Javier, A.Q.M. Murillo, R.Q. Baculi, Alpha-amylase conjugated biogenic silver nanoparticles as innovative strategy against biofilm-forming multidrug resistant bacteria, *Biocatal. Agric. Biotechnol.* 29 (2020) 101784.
- [28] L. Gong, D. Feng, T. Wang, Y. Ren, Y. Liu, J. Wang, Inhibitors of α -amylase and α -glucosidase: potential linkage for whole cereal foods on prevention of hyperglycemia, *Food Sci. Nutr.* 8 (2020) 6320–6337.
- [29] H. Kashtoh, K.-H. Baek, New insights into the Latest Advancement in α -amylase inhibitors of plant Origin with anti-diabetic effects, *Plants* 12 (2023) 2944.
- [30] J.O. Unuofin, G.A. Otunola, A.J. Afolayan, In vitro α -amylase, α -glucosidase, lipase inhibitory and cytotoxic activities of tuber extracts of *Kedrostis africana* (L.) Cogn, *Heliyon* 4 (2018) e00810.
- [31] M. Gazali, O. Jolanda, A. Husni, Nurjanah, F.A.A. Majid, Zuriat, R. Syafitri, In Vitro α -amylase and α -glucosidase inhibitory activity of green Seaweed *Halimeda tuna* extract from the Coast of Lhok Bubon, *Aceh. Plants* 12 (2023) 393.
- [32] A.M. Dirir, M. Daou, A.F. Yousef, et al., A review of alpha-glucosidase inhibitors from plants as potential candidates for the treatment of type-2 diabetes, *Phytochemistry Rev.* 21 (2022) 1049–1079.

- [33] S.T. Assefa, E.-Y. Yang, S.-Y. Chae, M. Song, J. Lee, M.-C. Cho, S. Jang, Alpha glucosidase inhibitory activities of plants with Focus on common Vegetables, *Plants* 9 (2020) 2.
- [34] Y. Zhang, Y. Pan, J. Li, Z. Zhang, Y. He, H. Yang, P. Zhou, Inhibition on α -glucosidase activity and non-enzymatic Glycation by an anti-Oxidative Proteoglycan from *Ganoderma lucidum*, *Molecules* 27 (2022) 1457.
- [35] S.A. Alshehri, S. Wahab, S.S. Abullais, G. Das, U. Hani, W. Ahmad, M. Amir, A. Ahmad, G. Kandasamy, R. Vasudevan, Pharmacological Efficacy of *Tamarix aphylla*: a Comprehensive review, *Plants* 11 (2022) 118.
- [36] M.A. Tienda-Vázquez, E.M. Melchor-Martínez, J.H. Elizondo-Luévano, R. Parra-Saldívar, J.S. Lara-Ortiz, B. Luna-Sosa, C.Q. Scheckhuber, Antidiabetic plants for the treatment of type 2 diabetes mellitus and associated Bacterial infections, *Processes* 11 (2023) 1299.
- [37] A. Ali, M.I. Ali Shah, C. Fu, Z. Hussain, M.N. Qureshi, et al., Dihydropyrazole derivatives Act as potent α -amylase inhibitors and free Radical Scavengers: synthesis, Bioactivity evaluation, structure–activity relationship, ADMET, and molecular docking studies, *ACS Omega* 8 (2023) 20412–20422.
- [38] R.S. Cheke, V.M. Patil, S.D. Firke, J.P. Ambhore, I.A. Ansari, H.M. Patel, S.D. Shinde, V.R. Pasupuleti, M.I. Hassan, M. Adnan, et al., Therapeutic outcomes of isatin and its derivatives against Multiple diseases: recent developments in drug discovery, *Pharmaceuticals* 15 (2022) 272.
- [39] Z. Xu, S. Zhang, C. Gao, J. Fan, F. Zhao, Zao-Sheng Lv, L.-S. Feng, Isatin hybrids and their anti-tuberculosis activity, *Chin. Chem. Lett.* 28 (2017) 159–167.
- [40] M.A. Abdelrahman, H. Almahlhi, T. Al-Warhi, T.A. Majrashi, M.M. Abdel-Aziz, W.M. Eldehna, M.A. Said, Development of novel isatin-tethered Quinolines as anti-Tubercular agents against multi and Extensively drug-resistant *Mycobacterium tuberculosis*, *Molecules* 27 (2022) 8807.
- [41] F. Bonvicini, A. Locatelli, R. Morigi, A. Leoni, G.A. Gentilomi, Isatin Bis-Indole and Bis-Imidazothiazole hybrids: synthesis and antimicrobial activity, *Molecules* 27 (2022) 5781.
- [42] I. Irfan, A. Ali, B. Reddi, M.A. Khan, P. Hasan, S. Ahmed, A. Uddin, M. Piatek, K. Kavanagh, Q.M.R. Haque, et al., Design, synthesis and Mechanistic studies of novel isatin-Pyrazole Hydrazone conjugates as selective and potent Bacterial MetAP inhibitors, *Antibiotics* 11 (2022) 1126.
- [43] R. Raj, C. Biot, S. Carrère-Kremer, L. Kremer, Y. Guérardel, J. Gut, P.-J. Rosenthal, D. Forge, V. Kumar, 7-Chloroquinoline–isatin conjugates: antimalarial, antitubercular, and cytotoxic evaluation, *Chem. Biol. Drug Des.* 83 (2014) 622–629.
- [44] A. Kumar, K. Lal, V. Kumar, M. Murtaza, S. Jaglan, A.K. Paul, S. Yadav, K. Kumari, Synthesis, antimicrobial, antibiofilm and computational studies of isatin-semicarbazone tethered 1,2,3-triazoles, *Bioorg. Chem.* 133 (2023) 106388.
- [45] S. Emami, M. Valipour, F.K. Komishani, F. Sadati-Ashrafi, M. Rasoulian, M. Ghasemian, M. Tajbakhsh, P.H. Masihi, A. Shakiba, H. Irannejad, N. Ahangar, Synthesis, in silico, in vitro and in vivo evaluations of isatin aroylhydrazones as highly potent anticonvulsant agents, *Bioorg. Chem.* 112 (2021) 104943.
- [46] S. Firke, R. Cheke, V. Ugale, S. Khadse, M. Gagarani, S.B. Surana, Rationale design, synthesis, and pharmacological evaluation of isatin analogues as antiseizure agents, *Letts. Drug Des. Discov.* 18 (2021) 1.
- [47] A.G. Bharathi Dileepan, T. Daniel Prakash, A. Ganesh Kumar, P. Shameela Rajam, V. Violet Dhayabaran, R. Rajaram, Isatin based macrocyclic Schiff base ligands as novel candidates for antimicrobial and antioxidant drug design: in vitro DNA binding and biological studies, *J. Photochem. Photobiol. B Biol.* 183 (2018) 191–200.
- [48] A. El-Faham, W.N. Hozzein, M.A.M. Wadaan, S.N. Khattab, H.A. Ghabbour, H.-K. Fun, M.R. Siddiqui, Microwave synthesis, Characterization, and antimicrobial activity of some novel isatin derivatives, *J. Chem.* 2015 (2015) 716987.
- [49] F. Bonvicini, A. Locatelli, R. Morigi, A. Leoni, G.A. Gentilomi, Isatin Bis-Indole and Bis-Imidazothiazole hybrids: synthesis and antimicrobial activity, *Molecules* 27 (2022) 5781.
- [50] M.A. Yousef, A.M. Ali, W.M. El-Sayed, W.S. Qayed, H.H.A. Farag, T. Aboul-Fadl, Design and synthesis of novel isatin-based derivatives targeting cell cycle checkpoint pathways as potential anticancer agents, *Bioorg. Chem.* 105 (2020) 104366.
- [51] W.M. Eldehna, A. Nocentini, S.T. Al-Rashod, G.S. Hassan, H.M. Alkahtani, A.A. Almhizia, A.M. Reda, H.A. Abdel-Aziz, C.T. Supuran, Tumor-associated carbonic anhydrase isoform IX and XII inhibitory properties of certain isatin-bearing sulfonamides endowed with in vitro antitumor activity towards colon cancer, *Bioorg. Chem.* 81 (2018) 425–432.
- [52] P. Czeleń, A. Skotnicka, B. Szeffler, Designing and synthesis of new isatin derivatives as potential CDK2 inhibitors, *Int. J. Mol. Sci.* 23 (2022) 8046.
- [53] S. Chowdhary, Shalini, A. Arora, V. Kumar, A Mini review on isatin, an anticancer scaffold with potential activities against Neglected Tropical diseases (NTDs), *Pharmaceuticals* 15 (2022) 536.
- [54] I. Abbasi, H. Nadeem, A. Saeed, H.A. Ali Khari, M.N. Tahir, M.M. Naseer, Isatin-hydrazone conjugates as potent α -amylase and α -glucosidase inhibitors: synthesis, structure and invitro evaluations, *Bioorg. Chem.* 116 (2021) 105385.
- [55] S.E. Nikoulina, T.P. Ciaraldi, S. Mudaliar, L. Carter, K. Johnson, R.R. Henry, Inhibition of glycogen synthase kinase 3 improves insulin action and glucose metabolism in human skeletal muscle, *Diabetes* 51 (2022) 2190–2198.
- [56] R.R. Ezzeldin, M.A. Saleh, S.A. Alwarsh, A. Rushdi, A.A. Althoqapy, H.S. El Saeed, A. Abo Elmaaty, Design and synthesis of novel 5-(3-(Trifluoromethyl) piperidin-1-yl)sulfonylindoline-2,3-dione derivatives as promising Antiviral agents: in vitro, in silico, and structure–activity relationship studies, *Pharmaceuticals* 16 (2023) 1247.
- [57] V.S. Pawar, D.K. Lokwani, S.V. Bhandari, K.G. Bothara, T.S. Chitre, T.L. Devale, N.S. Modhave, J.K. Parikh, Design, docking study and ADME prediction of Isatin derivatives as anti-HIV agents, *Med. Chem. Res.* 20 (2011) 370–380.
- [58] S.N. Pandeya, D. Sriram, G. Nath, E. de Clercq, Synthesis, antibacterial, antifungal and anti-HIV evaluation of Schiff and Mannich bases of isatin and its derivatives with triazole, *Arzneimittelforschung* 50 (2000) 55–59.
- [59] H.S. Al-Salem, M. Arifuzzaman, H.M. Alkahtani, A.N. Abdalla, I.S. Issa, A. Alqathama, F.S. Albalawi, A.F.M.M. Rahman, A series of isatin-Hydrazones with cytotoxic activity and CDK2 kinase inhibitory activity: a potential type II ATP competitive inhibitor, *Molecules* 25 (2020) 4400.
- [60] Alanazi, M.M., Alanazi, A.S. Novel 7-Deazapurine Incorporating isatin hybrid compounds as protein kinase inhibitors: (2023). Design, synthesis, in silico studies, and Antiproliferative evaluation. *Molecules* 28, 5869..
- [61] I.M.M.M. Othman, H. Mahross, M.A.M. Gad-Elkareem, M. Rudrapal, N. Gogoi, D. Chetia, K. Aouadi, M. Snoussi, A. Kadri, Toward a treatment of antibacterial and antifungal infections: design, synthesis and in vitro activity of novel arylhydrazothiazolylsulfonamides analogues and their insight of DFT, docking and molecular dynamic simulations, *J. Mol. Struct.* 1243 (2021) 130862.
- [62] R. Badraoui, T. Rebai, S. Elkahoui, M. Alreshidi, V. N. Veetil, E. Noumi, K. A. Al-Motair, K. Aouadi, A. Kadri, V. De Feo, et al., Allium subhirsutum L. As a potential Source of antioxidant and anticancer Bioactive molecules: HR-LCMS Phytochemical profiling, in vitro and in vivo pharmacological study, *Antioxidants* 9 (2020) 1003.
- [63] I.M.M. Othman, M.A.M. Gad-Elkareem, E.H. Anouar, K. Aouadi, A. Kadri, M. Snoussi, Design, synthesis ADMET and molecular docking of new imidazo[4,5-b]pyridine-5-thione derivatives as potential tyrosyl-tRNA synthetase inhibitors, *Bioorg. Chem.* 102 (2020) 104105.
- [64] A. Kadri, Z. Zarai, I.B. Chobba, N. Gharsallah, M. Damak, A. Békir, Chemical composition and in vitro antioxidant activities of *Thymelaea hirsuta* L: essential oil from Tunisia, *Afr. J. Biotechnol.* 10 (2011) 2930–2935.
- [65] F. Alminderej, S. Bakari, T.I. Almundarij, M. Snoussi, K. Aouadi, A. Kadri, Antimicrobial and wound healing potential of a new Chemotype from *Piper cubeba* L. Essential oil and in silico study on *S. aureus* tyrosyl-tRNA synthetase protein, *Plants* 10 (2021) 205.
- [66] K. Aouadi, E. Jeanneau, M. Msadek, J.-P. Praly, New Synthetic Routes toward enantiopure (2S,3R,4R)-4-Hydroxyisoleucine by 1,3-dipolar cycloaddition of a Chiral nitron to C4 alkenes, *Synthesis* 21 (2007) 3399–3405.
- [67] J. Brahmi, S. Ghannay, S. Bakari, K. Aouadi, A. Kadri, M. Msadek, S. Vidal, Unprecedented stereoselective synthesis of 3-methylisoxazolidine-5-aryl-1,2,4-oxadiazoles via 1,3-dipolar cycloaddition and study of their in vitro antioxidant activity, *Synth. Commun.* 46 (2016) 2037–2044.
- [68] S. Ghannay, S. Bakari, M. Msadek, S. Vidal, A. Kadri, K. Aouadi, Design, synthesis, molecular properties and in vitro antioxidant and antibacterial potential of novel enantiopure isoxazolidine derivatives, *Arab. J. Chem.* 13 (2020) 2121–2131.
- [69] I.M.M. Othman, M.A.M. Gad-Elkareem, E.H. Anouar, M. Snoussi, K. Aouadi, A. Kadri, Novel fused pyridine derivatives containing pyrimidine moiety as prospective tyrosyl-tRNA synthetase inhibitors: design, synthesis, pharmacokinetics and molecular docking studies, *J. Mol. Struct.* 1219 (2020) 128651.
- [70] I.M.M. Othman, M.A.M. Gad-Elkareem, E.H. Anouar, K. Aouadi, A. Kadri, M. Snoussi, Design, synthesis ADMET and molecular docking of new imidazo[4,5-b]pyridine-5-thione derivatives as potential tyrosyl-tRNA synthetase inhibitors, *Bioorg. Chem.* 102 (2020) 104105.

- [71] S. Ghannay, M. Snoussi, S. Messaoudi, A. Kadri, K. Aouadi, Novel enantiopure isoxazolidine and C-alkyl imine oxide derivatives as potential hypoglycemic agents: design, synthesis, dual inhibitors of α -amylase and α -glucosidase, ADMET and molecular docking study, *Bioorg. Chem.* 104 (2020) 104270.
- [72] A. Kadri, K. Aouadi, In vitro antimicrobial and α -glucosidase inhibitory potential of enantiopure cycloalkylglycine derivatives: Insights into their in silico pharmacokinetic, druglikeness, and medicinal chemistry properties, *J. Appl. Pharmaceut. Sci.* 10 (2020) 107–115.
- [73] N. Bouali, M. Ben Hammouda, I. Ahmad, S. Ghannay, A. Thouri, A. Dbeibia, H. Patel, W.S. Hamadou, K. Hosni, M. Snoussi, et al., Multifunctional derivatives of Spiropyrrolidine tethered Indeno-Quinoxaline heterocyclic hybrids as potent antimicrobial, antioxidant and antidiabetic agents: design, synthesis, in vitro and in silico approaches, *Molecules* 27 (2022) 7248.
- [74] H.A. Radwan, I. Ahmad, I.M.M. Othman, M.A.M. Gad-Elkareem, H. Patel, K. Aouadi, M. Snoussi, A. Kadri, Design, synthesis, in vitro anticancer and antimicrobial evaluation, SAR analysis, molecular docking and dynamic simulation of new pyrazoles, triazoles and pyridazines based isoxazole, *J. Mol. Struct.* 1264 (2022) 133312.
- [75] M. Ben Hammouda, S. Boudriga, K. Hamden, M. Askri, M. Knorr, C. Strohmann, L. Brieger, A. Krupp, E.H. Anouar, M. Snoussi, K. Aouadi, A. Kadri, New spiropyrrlothiazole derivatives bearing an oxazolone moiety as potential antidiabetic agent: design, synthesis, crystal structure, Hirshfeld surface analysis, ADME and molecular docking studies, *J. Mol. Struct.* 1254 (2022) 132398.
- [76] A. Ghabi, J. Brahmī, F. Alminderej, S. Messaoudi, S. Vidal, A. Kadri, K. Aouadi, Multifunctional isoxazolidine derivatives as α -amylase and α -glucosidase inhibitors, *Bioorg. Chem.* 98 (2020) 103713.
- [77] F. AlHawday, F. Alminderej, S. Ghannay, B. Hammami, A.E.A.E. Albadri, A. Kadri, K. Aouadi, In silico design, synthesis and evaluation of novel enantiopure isoxazolidines as dual α -amylase and α -glucosidase promising inhibitors, *Molecules* 29 (2024) 305.
- [78] E. Noumi, I. Ahmad, M. Adnan, A. Merghni, H. Patel, N. Haddaji, N. Bouali, K.F. Alabbosh, S. Ghannay, K. Aouadi, et al., GC/MS profiling, antibacterial, anti-Quorum sensing, and antibiofilm properties of *Anethum graveolens* L. Essential oil: molecular docking study and in-silico ADME profiling, *Plants* 12 (2023) 1997.
- [79] G. Froidi, F. Benetti, A. Mondin, M. Roverso, E. Pangrazzi, F.M. Djeujo, P. Pastore, *Pterodon emarginatus* seed Preparations: Antiradical activity, Chemical Characterization, and in silico ADMET parameters of β -caryophyllene and Farnesol, *Molecules* 28 (2023) 7494.
- [80] M.M. Fakhry, A.A. Mattar, M. Alsulaimany, E.M. Al-Olayan, S.T. Al-Rashood, H.A. Abdel-Aziz, New Thiazolyl-Pyrazoline derivatives as potential dual EGFR/HER2 inhibitors: design, synthesis, anticancer activity evaluation and in silico study, *Molecules* 28 (2023) 7455.
- [81] P. Czeleń, T. Jeliński, A. Skotnicka, B. Szefer, K. Szuprzycki, ADMET and Solubility analysis of new 5-Nitroisatine-based inhibitors of CDK2 enzymes, *Biomedicines* 11 (2023) 3019.
- [82] Y.O. Bouone, A. Bouzina, N.-E. Aouf, Synthesis, molecular docking analysis, ADMET and drug likeness prediction of a Benzenesulfonamide derivative analogue of SLC-0111, *Med. Sci. Forum* 14 (2022) 24.
- [83] N. Sepehri, H. Azizian, R. Ghadimi, et al., New 4,5-diphenylimidazole-acetamide-1,2,3-triazole hybrids as potent α -glucosidase inhibitors: synthesis, in vitro and in silico enzymatic and toxicity evaluations, *Monatsh. Chem.* 152 (2021) 679–693.
- [84] D.G. Aguila-Muñoz, G. Vázquez-Lira, E. Sarmiento-Tlale, M.C. Cruz-López, F.E. Jiménez-Montejo, V.E. López y López, C.H. Escalante, D. Andrade-Pavón, O. Gómez-García, J. Tamariz, et al., Synthesis and molecular docking studies of Alkoxy- and Imidazole-Substituted Xanthenes as α -amylase and α -glucosidase inhibitors, *Molecules* 28 (2023) 4180.
- [85] F. Alminderej, S. Ghannay, M.O. Elsamani, F. Alhawday, A.E.A.E. Albadri, S.E.I. Elbehairi, M.Y. Alfai, A. Kadri, K. Aouadi, In vitro and in silico evaluation of Antiproliferative activity of new isoxazolidine derivatives targeting EGFR: design, synthesis, cell cycle analysis, and Apoptotic Inducers, *Pharmaceuticals* 16 (2023) 1025.
- [86] B. Morak-Młodawska, M. Jeleń, E. Martula, R. Korlacki, Study of Lipophilicity and ADME properties of 1,9-Diazaphenothiazines with anticancer action, *Int. J. Mol. Sci.* 24 (2023) 6970.
- [87] S. Deb, A.A. Reeves, R. Hopefl, R. Bejusca, ADME and pharmacokinetic properties of Remdesivir: its drug interaction potential, *Pharmaceuticals* 14 (2021) 655.
- [88] S. Ouahabi, E.H. Loukili, A. Elbouzidi, M. Taibi, M. Bouslamti, H.-A. Nafidi, A.M. Salamatullah, N. Saidi, R. Bellaouchi, M. Addi, et al., Pharmacological properties of Chemically characterized extracts from Mastic tree: in vitro and in silico assays, *Life* 13 (2023) 1393.